MATHEMATICAL MODELING FOR PHAGOCYTE TRANSMIGRATION AND REVERSE ENGINEERING

by

MIN GON KANG

Presented to the Faculty of the Graduate School of
The University of Texas at Arlington in Partial Fulfillment
of the Requirements
for the Degree of

MASTER OF SCIENCE IN COMPUTER SCIENCE

THE UNIVERSITY OF TEXAS AT ARLINGTON

August 2010

To my wife Kyung-Hwa, and my parents made me who I am.

ACKNOWLEDGEMENTS

I would like to express my immeasurable gratitude to my advisor, Dr. Jean Gao, for her guidance, advice and support to reach my goal through my graduate studies. She encouraged me patiently to achieve my research successfully and develop creative thinking. I would also like to thank my exceptional committee, Dr. Chris Ding and Dr. Nikola Stojanovic, for sacrificing their time.

I wish to extend my thanks to collaborators, Dr. Liping Tang, for allowing me to use their data sets and helping me to develop my background in Phagocyte Transmigration.

I am grateful to Biocomputing and Vision Lab members and my friends who were always willing to help and give their best suggestions through the good times and bad times. Especially, Dr. Thakoor helped me achieve the part of optimal estimation and computing. Also countless discussion with Dongchul, Shuo, and Adel has given important inspiration to make a new algorithm.

Finally, I would like to thank my wife Kyung-Hwa for her constant love, support and encouragement. I am also very grateful to my parents, sister and my wife's family for their endless supports. This thesis would not have been possible without their helps.

July 1, 2010

ABSTRACT

MATHEMATICAL MODELING FOR PHAGOCYTE TRANSMIGRATION AND REVERSE ENGINEERING

MIN GON KANG, M.S.

The University of Texas at Arlington, 2010

Supervising Professor: Jean Gao

Computational modeling and simulation have been used as an important tool to analyze the behavior of a complex biology system. Typically, the biology system is a complex non-linear system where a large number of components are involved. One of the major obstacles in computational modeling and simulation is to determine a large number of parameters in the mathematical equations representing biological properties of the system.

To tackle this problem, we have developed a global optimization method, called Discrete Selection Levenberg-Marquardt (DSLM), for parameter estimation. The method uses a non-linear least square approach to approximate the solution of over-determined systems. For fast computational convergence, DSLM suggests a new approach for the selection of optimal parameters in the discrete spaces, while other global optimization methods such as genetic algorithm and simulated annealing use heuristic approaches that do not guarantee the convergence.

As a specific application example, we have targeted understanding phagocyte transmigration which is involved in the fibrosis process for biomedical device implan-

tation. The goal of computational modeling is to construct an analyzer to understand the nature of the system. Also, the simulation by computational modeling for phagocyte transmigration provides critical clues to recognize current knowledge of the system and to predict yet-to-be observed biological phenomenon.

TABLE OF CONTENTS

LIST OF FIGURES

LIST OF TABLES

CHAPTER 1

INTRODUCTION

Computational modeling and simulation have been highlighted in biomedical research for decades due to biologic systems' complexity and intractability by human. Computational modeling and quantitative simulation have played an important role in not only discovering biologic components' nature but also providing quantitative prediction. Generally, mathematical modeling is built based upon biologic experiments and background knowledge in biologic systems. The biological model is computed by several steps including hypothesis, computational estimation for the fittest model, and verification from experiment data. It is also called Reverse Engineering in biological area.

In this thesis, the mathematical modeling of phagocyte transmigration, which is one of the processes involved in fibrosis formed around an implanted biomedical device, is conducted, and a new solution for parameter estimation of the dynamic system is proposed for the accurate simulation of the biologic system.

Deep understanding of the phagocyte transmigration will disclose the contributing components and predict the evolution of foreign body responses, which will eventually lead to reducing the failure rate of implantation. The goal of this thesis is to provide mathematical modeling for phagocyte transmigration and to suggest a new optimization method, Discrete Selection Levenberg-Marquardt Algorithm (DSLM), to estimate optimal parameters of the mathematical equations for the fittest model to the data. It was assumed that the new method should be satisfied with global non-linear optimization solution and computational convergence in feasible time.

The background of phagocyte transmigration is introduced in Chapter 2. The modeling technique and the final mathematic modeling equations for phagocyte transmigration are presented in Chapter 3. For the estimation of parameters of the mathematical model, in Chapter 4 we introduce several methods currently used to solve non-linear least square problems and propose the new DSLM algorithm. In Chapter 5, the simulated results in a variety of biological environments are shown. The thesis closes with discussion and future work in Chapter 6.

CHAPTER 2

BIOMATERIAL-MEDIATED FIBROTIC RESPONSES

2.1 Preliminaries of Biomaterial-Mediated Fibrotic Responses

Due to remarkable development and increasing demand of medical implants such as breast implants, encapsulated tissues/cells, neural electrodes, and eye implants, medical implants are becoming more common. However, the increasing number of medical implants failure also has been reported. Medical implants provoke unpredicted responses and reactions of the immune system, which is fibrotic capsule formation surrounding the medical device. In earlier studies [1], [2], it is well documented that excessive fibrotic responses are responsible for the failure of many medical implants. In-depth understanding of the mechanism governing the reactions can play an important role in successful implantation and development of the biomaterial while reducing its side effects and simultaneously improving the functionality of the implants.

In 1998, Tang et al had conducted experiments [3] to recognize components involved in foreign body reactions and to discover their responses and reactions. To summarize the current understanding from the research, the evolution of biomaterial-mediate inflammatory responses may be divided into following six consecutive events (Figure 2.1):

1. Phagocyte transmigration through the endothelial barrier,
2. Chemotaxis toward the implants,
3. Adherence to the biomaterial,
4. Phagocyte activation,

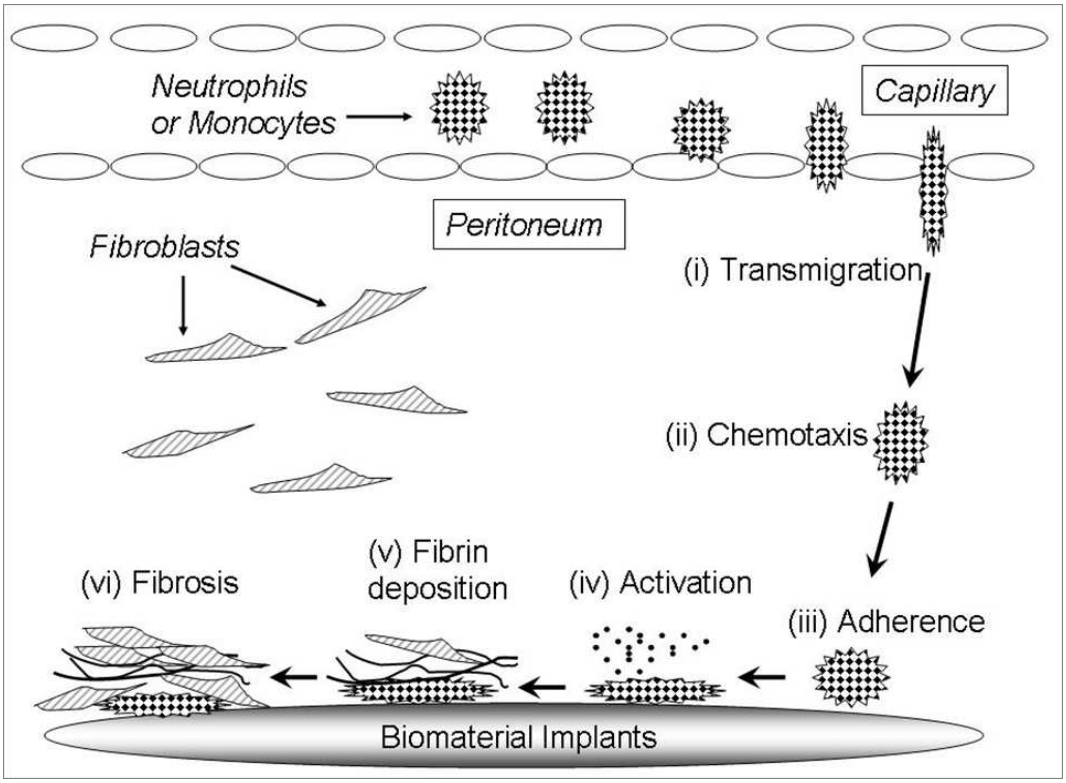

Figure 2.1: Hypothetical Sequence of Events Important in Fibrotic Responses to Implanted Biomaterials.

5. Fibrin deposition, and
6. Fibroblast proliferation and collagen production.

Briefly speaking, (1) after implantation, components involved in phagocyte transmigration such as mast cells, histamine, histamine receptors, and P/E selectins are activated to prompt phagocytes recruitment from capillary into peritoneum; (2) phagocytic cells transmigrated from capillary are mediated by certain chemokines which attract phagocytic cells toward implant surfaces; (3) receptors on cell surfaces interact with absorbed fibrinogen to bind between phagocytes and implant devices; (4) surface Fg triggers the activation of adherent phagocytes; (5) phagocyte-mediated fibrin is deposited on implants for localized formation of fibrin clot; (6) finally, fibrotic tissue forms surrounding biomaterial implants.

Among these six procedures, this thesis focuses on comprehensive modeling of phagocyte transmigration. It is assumed that certain components such as mast cells, histamine, histamine receptors, and P/E selectins, are involved in the event. The event was observed by evaluating the concentration' changing of polymorphonuclear neutrophils (PMN) and monocytesy/macrophages (MΦ) which are the most abundant type of phagocytes.

2.2 Hypothesis for Phagocyte Transmigration

Phagocyte transmigration is known as one of the major reactions of the immune system. After implantation, it prompts to recruit phagocytes from capillary to the peritoneal space where implants is located.

The previous study hypothesized that histamine might play an important role in the recruitment of inflammatory cells to implants. To verify the idea, histamine receptors, antagonist pyrilamine (an H1 receptor antagonist) and famotidine (an H2 receptor antagonist), were injected to implanted bio-materials in the mice. While neither receptor antagonists significantly reduced the accumulation of inflammatory cells on implant surfaces when given separately, combined treatment of H1 and H2 receptor antagonists dramatically decreased the number of phagocytes on implant surfaces as well as the number of PMN and MΦ recruited *de novo* to the peritoneal cavity. Therefore, it is legitimate to assume that histamine enhances phagocyte transmigration via both H1 and H2 receptors.

Mast cells are known for the majority source of histamine, although MΦ is also reported to produce and release histamine. There are a large amount of mast cells in the peritoneal space, and mast cells have the largest amount of histamine. Figure 2.2 [4] describes the degranulation in mast cells, which is the cellular process that mast cells release histamine. This hypothesis that mast cells influence histamine

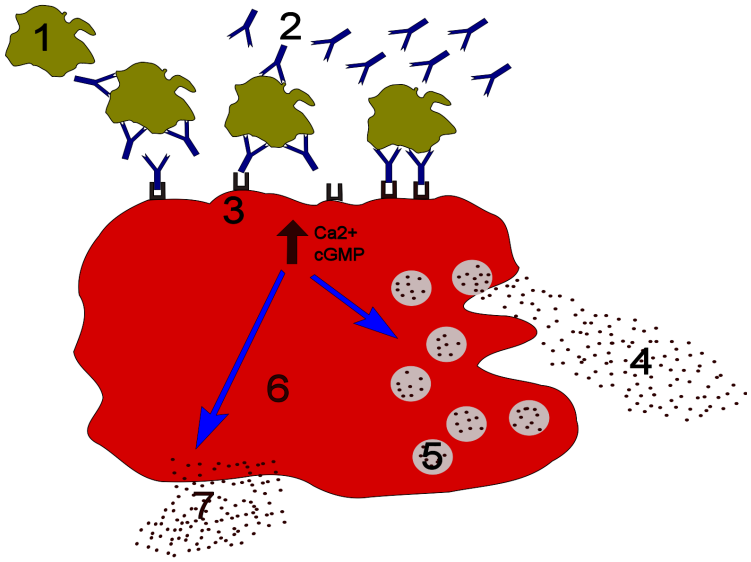

Figure 2.2: The Degranulation Process in A Mast Cell. 1 = Antigen; 2 = LgE; 3 = Fcε; 4 = Preformed Mediators (Histamine, Proteases, Chemokines, Heparin); 5 = Granules; 6 - Mast Cell; 7 - Newly Formed Mediators [4]

releasing, was clarified by the experiment using mast cell-deficient mice [3]. For the experiment, PET Disks were implanted into two groups of mice - normal mice and mast cell-deficient mice. Residual histamine is granules in mast cells to be about to be released as histamine. Residual histamine was measured to approximately estimate the degree of histamine from the two groups of mice, because the half-life of histamine is very short. In conclusion, the number of totally recruited phagocytes surrounding implants was significantly decreased for mast cells deficient mice comparing to normal mice.

It is reported that histamine augments the expression of P and E selectins [3], which are important cause of phagocytes' rolling and adhesion on endothelial cells. To verify the hypothesis that expression of P and E selectins might facilitate the transmigration of phagocyte through the endothelial barrier, experiments using P selectin-deficient mice, E selectin-deficient mice, and both P and E selectins-deficient

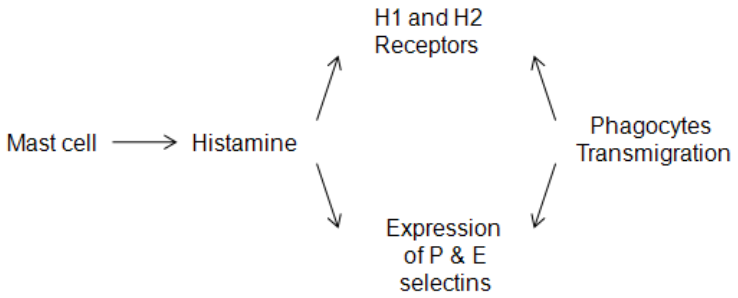

Figure 2.3: Flowchart of Phagocyte Transmigration [6]

mice were carried out [5]. As a result, significant reduction of phagocyte recruitment and adhesion were observed on P/E double knock out mice.

For these hypotheses and experiments, it is believed that components of the system - mast cells, histamine, histamine receptors, and P/E selectins - are involved in the process of phagocyte transmigration with their actions, as shown in Figure 2.3.

Under the current knowledge, computational modeling was attempted for Phagocyte Transmigration by Xue et al [6], [7]. Xue approached modeling of the system with the concept of a dynamic system and control theory. However, although the computational modeling represents the quantitative evolution of the system's components appropriately and predicts the future degrees, some biological background for residual histamine part were overlooked and the method of parameter estimation for exact simulation was not shown. Therefore, this thesis focuses on modeling the system with mathematical interpretation of biological behaviors under deeper-understanding of the biologic phenomenon and suggests a new algorithm to estimate parameters of the modeling equations for the fittest modeling to real experiment data.

CHAPTER 3

COMPUTATIONAL MODELING

3.1 Computational Modeling

In the previous Chapter, biologic hypotheses of phagocyte transmigration were built. In summery, the consecutive events are taken place in phagocyte transmigration in the order as: (1) mast cells somehow get stimulated and become active immediately after implantation; (2) activated mast cells release histamine; (3) histamine behavior is stimulated by combining with histamine receptors; (4) histamine receptors exert capillary vessel to increase its permeability for phagocyte to transmigrate into peritoneal space; (5) P and E selectins prompted by histamine stimulate rolling and adhesion of phagocyte on endothelial cells of capillary; (6) when reaching a certain level of capillary permeability, phagocytes start transmigration into peritoneal space, as shown as Figure 3.1. In this section, the mathematical equations are derived from the biologic hypotheses in order to simulate the system and to predict the degree of the components involved in phagocyte transmigration.

3.1.1 Phagocyte Transmigration as a Dynamic System

In control theory, systems consist of a finite number of variables, $x_1, \ldots, x_n$, called the "state". The mathematical form for a non-linear system is given by a differential equation system of the type:

$$\dot{\mathbf{x}} = f(t, \mathbf{x}, \mathbf{u}), \tag{3.1}$$

$$\mathbf{y} = h(t, \mathbf{x}, \mathbf{u}), \tag{3.2}$$

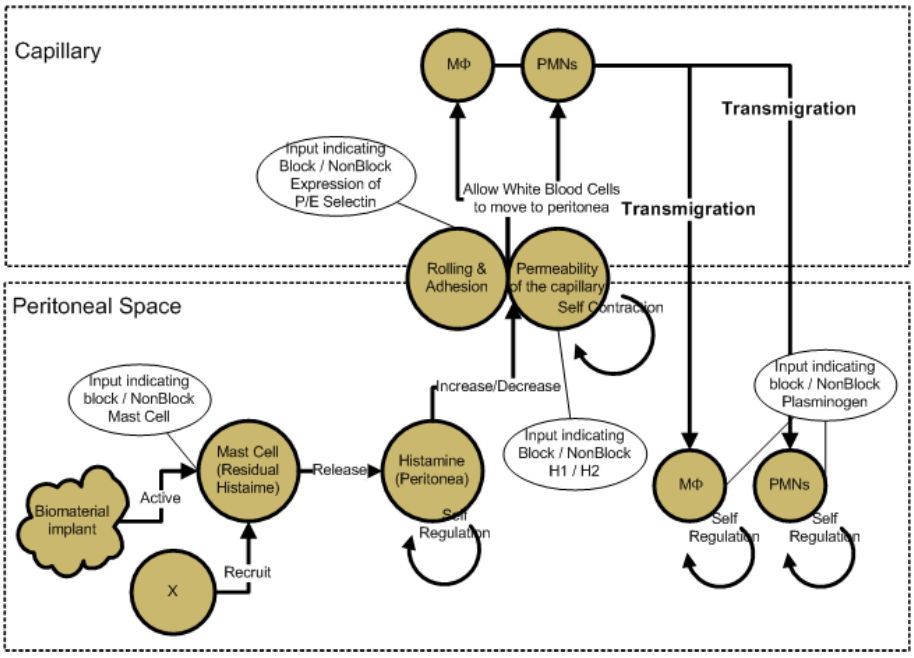

Figure 3.1: System Organization for Phagocyte Transmigration

where $\mathbf{x}$ is the state vector of dimension n, f and h are the functions of the state and control variables, $\mathbf{u}$ is the input variable of dimension m, $\mathbf{y}$ is the output vector of dimension p. The system requires the assumption - the initial condition is known so that differential equations propagate the evolution of the system with the initial variables.

3.1.1.1 Residual Histamine

As mentioned in the previous chapter, residual histamine measured to approximately estimate histamine due to the difficulty of direct measurement of histamine. However, residual histamine is immature granules in mast cells, and residual histamine might strongly affect histamine releasing. Therefore, residual histamine was considered as a major component instead of mast cells.

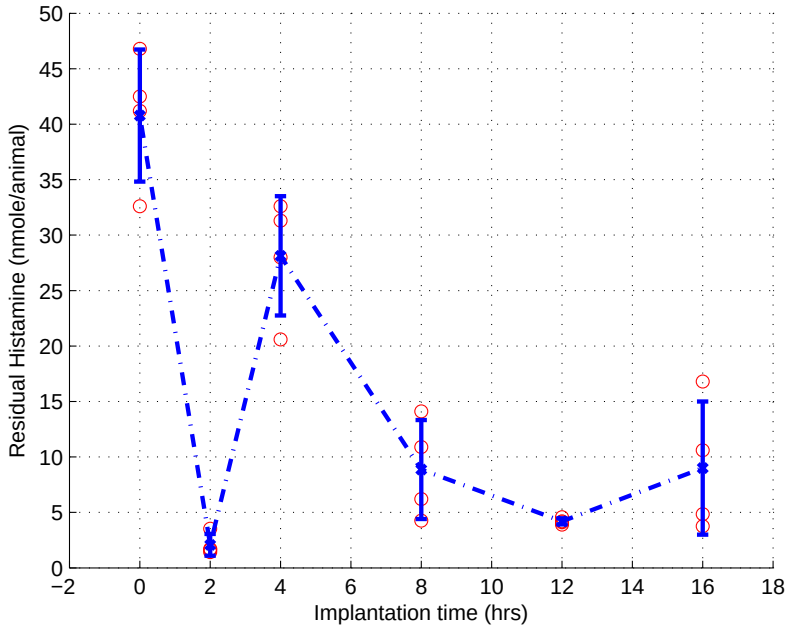

Figure 3.2: Experiment Data for Residual Histamine

According to the experiment data shown in Figure 3.2, it is shown that releasing of residual histamine may have a regular pattern. Xue [6] designed a model using damped harmonic oscillator:

$$\ddot{C}_{hmr}(t) + q\dot{C}_{hmr}(t) + \omega^2(t)C_{hmr}(t) = 0, \tag{3.3}$$

where C_{hmr} is released histamine, $\omega(t)$ indicates the oscillator frequency, and q is the damped parameter.

However, the approach to this modeling does not seem to be based on biologic knowledge. In biological sense, the phenomenon that residual histamine decreases up to the first two hours can be described as residual histamine's degranulation from mast cells for histamine releasing. In addition, another legitimate assumption that the number of new mast cells is dramatically increased by some unknown external

source after two hours may be persuasive. In the reason, the external source was modeled by a damped harmonic oscillator,

$$\ddot{U}_{xrmc}(t) + 2\beta\dot{U}_{xrmc}(t) + \omega_0^2(t)U_{xrmc}(t) = 0, \tag{3.4}$$

where U_{xrmc} is the function of the external input source to release new mast cells, β is a non-negative constant for resistance of friction and mass. When $\beta < w_0$, it is called *under damped oscillation*. The solution is [8]

$$U_{xrmc}(t) = \exp(-\beta t)(x_0 \cos w_1 t + \tfrac{\beta w_0 + v_0}{w_1} \sin w_1 t), \tag{3.5}$$
$$w_1 = \sqrt{w_0^2 - \beta^2},$$

Here, we assume $x_0 = 0, \frac{\beta w_0 + v_0}{w_1} = A$ (a constant for simple), and shift the sine function as much as $\frac{\pi}{2}$ to match with the experimental result. In addition, because the function must be positive, it is lifted up as much as A to make itself always positive.

$$U_{xrmc}(t) = A + A\exp(-\beta t)\cos(\sqrt{1-\beta^2}\omega_0 t) \tag{3.6}$$

Moreover, in order to fit with the graph shape of residual histamine more exactly, constant A and w_0 were transformed to negative exponential function and variables t was changed to $(t - t_1)$. The final form is

$$U_{xrmc}(t) = A(t) + A(t)\exp(-\beta(t-t_1))\cos(\sqrt{1-\beta^2}\omega_0(t)(t-t_1)), \tag{3.7}$$

$$A(t) = k_{e0}\exp(-k_{k1}(t-t_1)), \tag{3.8}$$

$$\omega_0(t) = k_{w0}\exp(-k_{k2}(t-t_1)), \tag{3.9}$$

where k_{e0} is the initial concentration of the eternal source, k_{k1} is the self contraction of the external source, k_{w0} is the initial value of oscillation frequency, k_{k2} is the contraction rate of oscillation frequency, t_1 is the starting point that the external source is released.

Basically, most biological components have a half-life cycle. In other words, it can model the system considering propagation and self regulation as conflicting contexts. In this sense, residual histamine can be modeled by the following equation.

$$\dot{C}_{rh}(t) = -k_{rhch}C_{rh}(t) + U_{xrmc}(t) \tag{3.10}$$

where $C_{rh}(t)$ is the concentration function of residual histamine, k_{rhch} is the rate that residual histamine decayed, $U_{xrmc}(t)$ is the input function defined above. The reason why propagation for residual histamine is not considered is only new mast cells determine the concentration of residual histamine. $U_{xrmc}(t)$ represents the external source that prompts mast cells' releasing.

3.1.1.2 Histamine

The concentration of histamine is increased as much as residual histamine's decreasing.

$$\dot{C}_h(t) = k_{rhch}C_{rh}(t)I_{mc}(t) - k_{hs}C_h(t) \tag{3.11}$$

where $C_h(t)$ is the concentration function of histamine, k_{rhch} is the rate that histamine released from residual histamine given from residual histamine equation (3.10), k_{hs} is the rate that histamine regulates itself, $I_{mc}(t)$ is an input parameter indicating block/non-block mast cells. The first term on the right hand side of Equation (3.11) represents the increasing of histamine released from mast cells. $I_{mc}(t)$ indicates the

concentration level of mast cells for knock-out experiment using mast cell deficient mice, where $0 \leq I_{mc}(t) \leq 1$. The second term on the right hand side of Equation (3.11) represents the decay of histamine itself.

3.1.1.3 Histamine Receptor

Histamine receptors enhance the permeability of the endothelial cell barrier of capillary for phagocyte to transmigrate into the peritoneal space. Histamine exerts its action only if combined with histamine receptors. The action is determined by histamine receptors - H1 histamine receptor or H2 histamine receptor. Therefore, the concentration of meaningful histamine receptors can be determined by the degree of histamine.

$$\dot{C}_{hr}(t) = \frac{k_{hchrt} C_h(t)}{k_{hchrb} + C_h(t)} - k_{hrs} C_{hr}(t) \tag{3.12}$$

where $C_{hr}(t)$ is the concentration function of histamine receptors, k_{hchrt} and k_{hchrb} are the rate bounds that histamine receptors are combined by histamine, k_{hrs} is the rate that histamine receptors regulate themselves. In the same way as histamine modeling, the first term on the right hand side represents increasing histamine receptors combined with histamine while the second term shows the decay rate of histamine receptors. However, it adopted a hyperbolic form for the first term unlike Equation 3.11. It sets a maximally increasable bound on change of histamine receptors because it would not increase unlimitedly.

3.1.1.4 Selectins

P and E selectins play an important role in phagocyte's rolling and adhesion on endothelial cells of capillary while histamine receptors prompt to increase permeability of capillary. As same as histamine receptors, P and E selectins are stimulated by

histamine. In other words, the concentration of histamine determines the quantity of P and E selections.

$$\dot{C}_s(t) = \frac{k_{hcst} C_h(t)}{k_{hcsb} + C_h(t)} - k_{ss} C_s(t), \tag{3.13}$$

where $C_s(t)$ is the concentration function of Selectins, k_{hcsb} and k_{hcst} are the rate bounds that Selectins are released by histamine for hyperbolic form, k_{ss} is the rate that Selectins regulate themselves

3.1.1.5 Phagocytes

PMN and MΦ are the most common phagocytes. The total recruited PMN and MΦ represent the concentration of transmigrated phagocyte into peritoneal space and surrounding implants. For modeling of PMN and MΦ, we consider capillary permeability for PMN and MΦ that represent the transmigration rate of phagocyte.

$$\dot{C}_{pmnp}(t) = \frac{k_{pmnipt} C_{hr}(t) C_s(t) I_{pmns}(t) I_{pmnhr}(t)}{k_{pmnipb} + C_{hr}(t) C_s(t) I_{pmns}(t) I_{pmnhr}(t)} - k_{pmnps} C_{pmnp}(t) \tag{3.14}$$

where $C_{pmnp}(t)$ is the capillary permeability function for PMN to move into peritonea, k_{pmnipb} and k_{pmnipt} are the rate bounds for histamine receptors and Selectins to increase permeability for PMN, $C_{hr}(t)$ is the concentration function of histamine receptors, $C_s(t)$ is the concentration function of Selectins, k_{pmnps} is the contraction rate of capillary permeability, $I_{pmnhr}(t)$ is the input indicating block/non-block histamine receptors, $I_{pmns}(t)$ is the input indicating block/non-block Selectins. Similarly, the permeability function for MΦ can be modeled as,

$$\dot{C}_{mpp}(t) = \frac{k_{mpipt} C_{hr}(t) C_s I_{mps}(t) I_{mphr}(t)}{k_{mpipb} + C_{hr}(t) C_s I_{mps}(t) I_{mphr}(t)} - k_{mpps} C_{mpp}(t), \tag{3.15}$$

where $C_{mpp}(t)$ is the capillary permeability function for MΦ to move into peritonea, k_{mpipb} and k_{mpipt} are the rate for histamine receptors and Selectins to increase permeability for MΦ, k_{mpps} is the contraction rate of capillary permeability. Now we can model the recruited PMN as,

$$\dot{C}_{pmn}(t) = C_{pmnp}(t) - k_{pmns}C_{pmn}(t), \tag{3.16}$$

where $C_{pmn}(t)$ is the concentration function of PMN, C_{pmnp} is the concentration of permeability for PMN, k_{pmns} is the rate that PMN self contraction. Now we can model the recruited MΦ as,

$$\dot{C}_{mp}(t) = C_{mpp}(t) - k_{mps}C_{mp}(t), \tag{3.17}$$

where $C_{mp}(t)$ is the concentration function of MΦ, C_{mpp} is the concentration of permeability for MΦ, k_{mps} is the rate that MΦ self contraction.

3.1.2 Discrete Equations

Differential equations are commonly used as mathematical modeling method to represent dynamic evolution of biological propagation. However, differential equations is difficult to compute accurate simulation and apply algorithms. Therefore, the most popular way is to convert differential equations to discrete equations of the type:

$$x_{n+1} = f(x_n, x_{n-1}, \ldots), x_0 = a_0 \tag{3.18}$$

A discrete equation needs an initial value for the first state, and it iterates computing next states recursively depending on previous state. Basically, the differential equa-

tion form can be represented in discrete-time with constant sampling interval $\triangle$t by [9]

$$\dot{y} = ay + bu(t), \tag{3.19}$$

$$y_{k+1} = \Phi y_k + \Gamma u_k, \tag{3.20}$$

where the integer constant k is the sample index, and

$$\Phi = e^{a\triangle t}, \tag{3.21}$$

$$\Gamma = \int_0^{\triangle t} be^{at}dt = \frac{b}{a}(e^{a\triangle t} - 1). \tag{3.22}$$

In this way, mathematical differential equations for the consecutive events during transmigration can be transformed to the following equations. For residual histamine,

$$C_{rh(k+1)} = e^{-k_{rhch}\triangle t}C_{rh(k)} - \frac{1}{k_{rhch}}(e^{-k_{rhch}\triangle t} - 1)U_{xrmc(k)}. \tag{3.23}$$

For histamine,

$$C_{h(k+1)} = e^{-k_{hs}\triangle t}C_{h(k)} - \frac{1}{k_{hs}}(e^{-k_{hs}\triangle t} - 1)k_{rhch}C_{rh(k)}I_{mc}(t). \tag{3.24}$$

For histamine receptors,

$$C_{hr(k+1)} = e^{-k_{rhs}\triangle t}C_{hr(k)} - \frac{1}{k_{rhs}}(e^{-k_{rhs}\triangle t} - 1)\frac{k_{hchrt}C_{h(k)}}{k_{hchrb} + C_{h(k)}}. \tag{3.25}$$

For P/E selectins,

$$C_{s(k+1)} = e^{-k_{ss}\triangle t}C_{s(k)} - \frac{1}{k_{ss}}(e^{-k_{ss}\triangle t} - 1)\frac{k_{hcst}C_{h(k)}}{k_{hcsb} + C_{h(k)}}. \tag{3.26}$$

For permeability of PMN,

$$C_{pmnp_{(k+1)}} = e^{-k_{pmnps}\triangle t} C_{pmnp_{(k)}} - \frac{1}{k_{pmnps}}(e^{-k_{pmnps}\triangle t} - 1)\frac{k_{pmnipt} C_{h(k)} C_{s(k)} I_{pmns}(t) I_{pmnhr}(t)}{k_{pmnipb} + C_{h(k)} C_{s(k)} I_{pmns}(t) I_{pmnhr}(t)}. \tag{3.27}$$

For PMN

$$C_{pmn_{(k+1)}} = e^{-k_{pmns}\triangle t} C_{pmn_{(k)}} - \frac{1}{k_{pmns}}(e^{-k_{pmns}\triangle t} - 1) C_{pmnp_{(k)}}. \tag{3.28}$$

For permeability of MΦ

$$C_{mpp_{(k+1)}} = e^{-k_{mpps}\triangle t} C_{mpp_{(k)}} - \frac{1}{k_{mpps}}(e^{-k_{mpps}\triangle t} - 1)\frac{k_{mpipt} C_{h(k)} C_{s(k)} I_{mps}(t) I_{mphr}(t)}{k_{mpipb} + C_{h(k)} C_{s(k)} I_{mps}(t) I_{mphr}(t)}. \tag{3.29}$$

For MΦ

$$C_{mp_{(k+1)}} = e^{-k_{mps}\triangle t} C_{mp_{(k)}} - \frac{1}{k_{mps}}(e^{-k_{mps}\triangle t} - 1) C_{mpp_{(k)}}. \tag{3.30}$$

The initial value of Equation (3.23) was set by the mean of the variables of observation data set at time 0, and initial values for other Equations (3.24), (3.25), (3.26), (3.27), (3.28), (3.29), (3.30) were set as 0 for simplification.

CHAPTER 4

PARAMETER ESTIMATION

4.1 Parameter Estimation for The Reverse Problems

In the previous chapter, we introduced computational modeling of biological components involved in phagocyte transmigration. As can be seen, a dynamic system often contain numerous parameters whose values indicate characteristics of the system. Thus, it has been believed that estimating parameters of the system is essential to discover component's behavior in the system and a successful computational modeling. However, they are often very difficult to determine.

Generally, parameter estimation is conducted by approximately minimizing the sum of errors between observation data set and predicted values by mathematical modeling equations under the assumption that the modeling represents the system appropriately. The parameters calculated by minimizing of the errors may represent the nature properties of the system's components best. It is called as *Reverse Problem* since it extracts the true model from the observation data set.

A least squares method is the standard approximate solution for reverse problems using minimizing the sum of squares of the errors between the observation data set and estimated variables of the model function. A data set consists of n points (t_i, $\tilde{y}_i$), $i = 1, \ldots, n$, where n is the number of data, t_i is an ith variable and $\tilde{y}_i$ is the observation. The unconstrained problems can be defined by the notation of fitting

a model to n pieces of observation using p parameters, given R:$\Re^p \rightarrow \Re^n$, if $R(\mathbf{x})$ is continuously differentiable. [10]

$$\min F(\mathbf{x}) = R(\mathbf{x})^\top R(\mathbf{x}) = \sum_{i=1}^{n} {r_i}^2 \tag{4.1}$$

R($\mathbf{x}$) is a residual function between model function's variables and the data set by observation, and

$$R(\mathbf{x}) = \tilde{y} - f(\mathbf{t}, \mathbf{p}), \tag{4.2}$$

$$r_i = \tilde{y_i} - f(t_i, \mathbf{p}) \tag{4.3}$$

where $\tilde{y_i}$ is the observation, $f(t_i, p)$ is the model function that has m number of parameters (i.e. p) corresponding to t_i. Here, the goal is to find optimal p, subject to minimization of F($\mathbf{x}$) function. Notice the first differential function of R(x) is defined as J($\mathbf{x}$) = $R'(\mathbf{x}) = (\partial_j r_i(\mathbf{x}))$, the gradient of $F(\mathbf{x})$ is

$$\nabla F(\mathbf{x}) = J(\mathbf{x})^\top R(\mathbf{x}), \tag{4.4}$$

4.2 Non-Linear Least Squares Algorithms

In this section, some popular algorithms for non-linear least squares and their definitions will be introduced before proposing a new algorithm, Discrete Selection Levenberg-Marquardt algorithm.

Solutions to least squares problems fall into two types - linear least squares solutions and non-linear least squares solutions. Unlike linear least square problems, most of non-linear least squares solutions used to refine processing iteratively with

the initial parameter as Equation (4.5) because there is no closed-form expression for the best-fitting parameters for non-linear least squares problems.

$$x^{k+1} = x^k + \Delta x \tag{4.5}$$

where k is an iteration number and Δx is the increment of x for each iteration. Equation (4.5) describes how to update its optimal approximation of parameters for each iteration. Algorithm 1 shows a general framework of non-linear least squares solutions [11].

Algorithm 1 General Framework of Non-Linear Least Squares Solutions

1: $k \leftarrow 0$
2: **repeat**
3: Find a descent direction h
4: $x^{k+1} \leftarrow x^k + \alpha h$
5: $k \leftarrow k + 1$
6: **until** Stop

Most iterative non-linear least squares solutions follow the framework shown in Algorithm 1. Only the difference of the approaches is the definition of α and h, which are the step size and the increment of x respectively, for line 4.

In 1669, Isaac Newton proposed Newton's Method [12] to find a minimum or maximum of function, $f(\mathbf{x})$, using the concept that the derivative of the function is zero at its minimum or maximum.

$$x^{k+1} = x^k - \frac{f'(x_k)}{f''(x_k)} \tag{4.6}$$

where $f(\mathbf{x})$ is a twice-differentiable function and it begins with initial guess x_0 which should be close enough to x^*. The form of Equation (4.6) is derived from the first derivative of the second order Taylor expansion of *f(x)*,

$$f(x + \Delta x) \approx f(x) + f'(x)\Delta x + \frac{1}{2}f''(x)\Delta x^2, \tag{4.7}$$

$$\frac{\partial f(x + \Delta x)}{\partial \Delta x} = f'(x) + f''(x)\Delta x = 0 \tag{4.8}$$

For the matrix space, it can be rewritten by

$$x^{k+1} = x^k - [Hf(x_k)]^{-1}\Delta f(x_k) \tag{4.9}$$

where H is Hessian matrix which is the square matrix of second-order partial derivatives of the function. As a result, Newton's method can converge quickly if the initial guess x_0 is close to x^*. However, it can, unfortunately, easily go to the wrong direction if initial guess x_0 is far from x^*. Another problem is that it is sometimes difficult to calculate Hessian matrix.

The steepest gradient method is a first-order optimization algorithm using gradient descent to find a local minimum or maximum. In Equation (4.5), the steepest gradient method defines

$$x^{k+1} = x^k - \alpha F'(x^k), \tag{4.10}$$

where α is fixed constant computed by line search. It finds an optimum quickly even though the initial guess is far from the optimum and the system size is very large. However, as it goes close to optimum, it can be infeasible since the step size α is fixed once.

Gauss-Newton algorithm remedies the shortcomings of both Newton method and the steepest gradient method. While Newton Method requires the second derivatives, Gauss-Newton algorithm doesn't. The second derivatives is defined by

$$\nabla^2 f(x) = J(x)^\top J(x) + \sum_{i=1}^{n} r_i(x)\nabla^2 r_i(x). \tag{4.11}$$

Gauss-Newton algorithm approximates the second derivatives as substituting it with square of the first derivative - $J(x)^\top J(x)$ which is the first term of (4.11) and ignoring the residual part of (4.11), since the residuals do not strengthen the nonlinearity. Therefore, $J(x)^\top J(x)$ can be a good Hessian approximation. For this reason, Equation (4.6) can be re-written by substituting the second derivatives,

$$(J_R(\mathbf{x})^\top J_R(\mathbf{x}))\triangle\mathbf{x} = -J_R(\mathbf{x})^\top R(\mathbf{x}) \tag{4.12}$$

where $J(x)^\top J(x)$ is symmetric and positive semi-definite. According to (4.2), (4.12) can be transformed as

$$(J_f(\mathbf{x})^\top J_f(\mathbf{x}))\triangle\mathbf{x} = J_f(\mathbf{x})^\top R(x) \tag{4.13}$$

As a result, Gauss-Newton algorithm seeks to find an optimal minimum updating the gradient of x with the form of (4.13) for each iteration. Gauss-Newton method has an advantage that it does not need the second derivatives, and it has quadratic final convergence if $\mathbf{x}$ close to $\mathbf{x}^*$. Generally, if f has small curve, it is expected to be super convergence. However, it may not have a good performance if curve of f'' varies slowly. That is because the second term of (4.11), which is ignored, strongly affects the function's non-linearity.

To improve limitations of of the steepest gradient method, Newton method, and Gauss-Newton method, Levenberg-Marquardt algorithm, which is currently the most popular method, is proposed by Levenberg [13] and Marquardt [14]. Levenberg-Marquardt algorithm[11] defines (4.13) of Gauss-Newton method as

$$(J_f(x)^\top J_f(x) + \mu I)\triangle x = J_f(x)^\top R(x) \tag{4.14}$$

where I is an identity matrix, μ is a positive scalar called *Marquardt damping parameter*. μI represents the second term of (4.11). Interestingly, the algorithm becomes Gauss-Newton method if μ is small, while it behaves like a steepest descent method when μ is large. In other words, if $\boldsymbol{x}$ is close to the solution, μ becomes small; and μ will be large when x is far from the solution. If μ is zero, it will be exactly the Gauss-Newton method. Hence, Levenberg-Marquardt algorithm is an adaptive algorithm to retain strength of the steepest gradient method, Newton method, and Gauss-Newton Method.

However, although Levenberg-Marquardt algorithm is robust to find an optimal minimum, it has a limitation of local optimization. In other words, it may fail to find the global minimum if it starts with initial x belongs to other local curves. In reality, local optimization is often not suitable to solve the non-linear problems in many cases due to non-convexity.

4.3 Discrete Selection Levenberg-Marqurdt

4.3.1 Introduction

Discrete Selection Levenberg-Marqurdt (DSLM) is motivated by the following considerations. Levenberg-Marquardt method converges quickly to the optimum solution. However, it tends to fall into the local optimum space that is the closest to

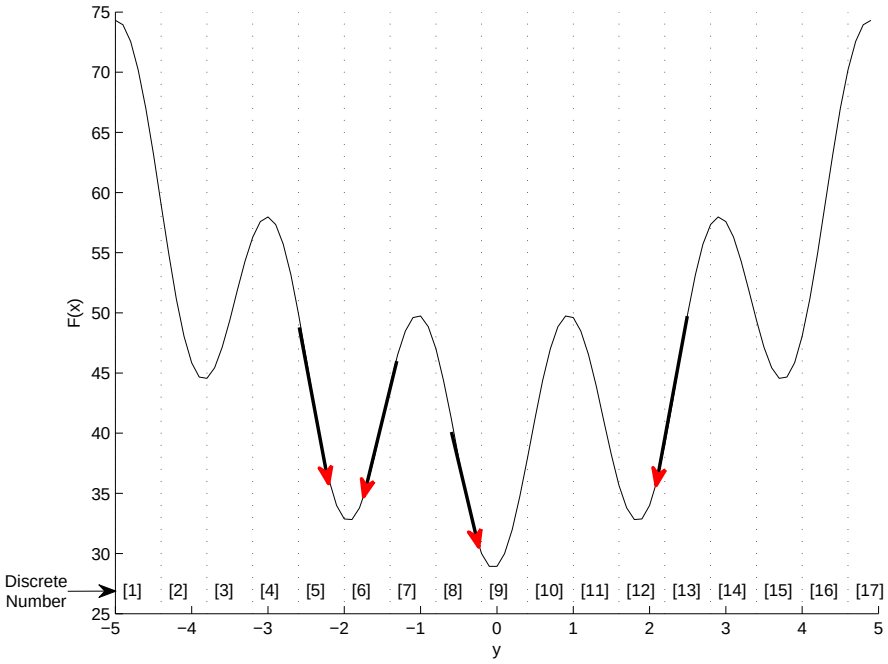

Figure 4.1: Levenberg-Marquardt Algorithm's Convergence for Rastrigin Function. [1], ..., [17] is A Number of Discrete Space. For Example, The Continuous Spaces Between -4 and -2 are Discrete as The Number of Discrete Space, [3], [4] and [5].

the initial guess, x_0, not the global optimum. Figure 4.1 describes how Levenberg-Marquardt algorithm converges with each different initial x_0. Hence, if it is possible to discretize the space to cover possibly every local curves with number N, Levenberg-Marquardt algorithm can be extended to a global algorithm searching local curves belong to the discrete space.

Typically, naive global optimizations are NP-hard problems because of dimension curse. Commonly, computational models may have scores of parameters. Hence, most of global optimizations such as Genetic algorithm adopt heuristic approach instead of a naive approach. DSLM seeks to search the global optima for each $\mathbf{x}$ dimension iteratively instead of comprehensive $\mathbf{x}$ dimensions which may lead unforeseeable computational cost. Its concept reduces the searching spaces to the linear.

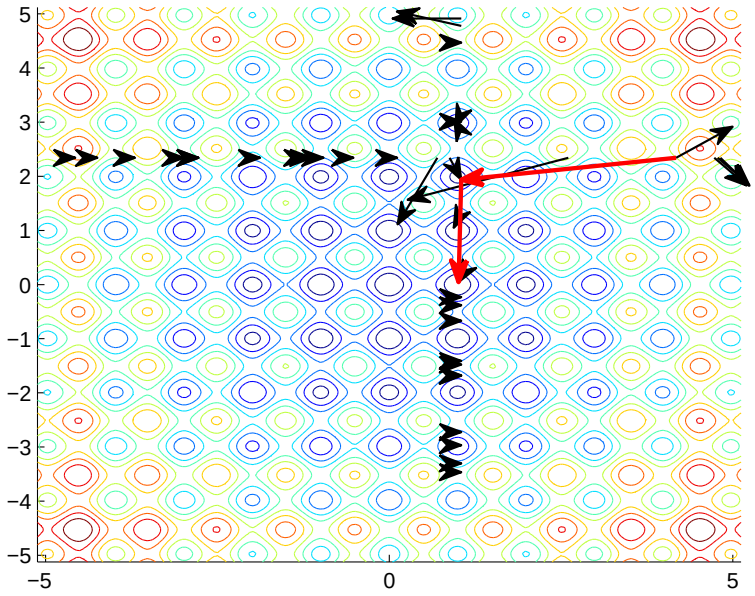

Figure 4.2: Flow of Discrete Selection Levenberg-Marquardt Algorithm

4.3.2 Selection

Like other non-linear least squares algorithms, DSLM starts with initial x_0 for iterative computing. Instead of seeking to converging to the local optima, DSLM attempts to vary the initial guesses within the dimension of each parameter fixing other parameters. Denote P_i is a finite vector to represent the space of the i^{th} parameter. While the global optimizations search the comprehensive spaces whose complexity is $P_1 \times P_2 \times \cdots \times P_n$, the complexity of searching space in DSLM becomes $P_1 + P_2 + \cdots + P_n$ because it searches iteratively each parameter space. Then, it checks the scores of the function calculated with updated x by conducting Levenberg-Marquardt method with them as the initial guesses. In Figure 4.2, the arrows show that it checks the scores of the function varying y dimension variables under the condition x dimension fixed for the 2-dimension space. The score of the function is calculated by the result that Levenberg-Marquardt algorithm converges to. Once it selects the optimal pa-

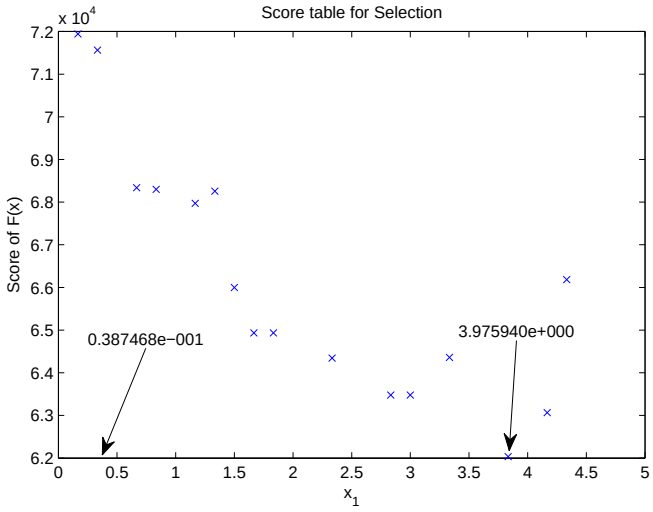

Figure 4.3: Score Table for Selection of Optimal Parameter in A Dimension for Residual Histamine Modeling

rameter that has the best function score in the dimension, the parameter is updated to the new parameter that Levenberg-Marquardt method converges. Then, it seeks to the next optimal parameters with fixed parameters previously chosen as the optimum. It iterates the selection process until parameters are converges. For example, Figure 4.3 depicts a score table of the discrete spaces(discretization will be explained next section) while computing DSLM algorithm for residual histamine modeling. It is computing the first parameter of x. The given initial parameter variable was 0.387468e-001. With 30 number of discrete spaces, it conducts Levenberg-Marquardt method for each discrete point to find its each local optimum. The x points of Figure 4.3 show the scores of the function for each discrete space. In this example, the parameter was updated to 3.975940e+000, which has the lowest score, while other parameters were updated to new values subject to moving toward to local optimum. Preciously, it may not optimal solution at the first iteration. However, it will be close to the optimal solution after iteratively updating the optimums of each parameter.

4.3.3 Discretization

Discretization of each parameter space is the key part to affect the performance and computational cost for DSLM algorithm. Given N numbers of discrete spaces of a parameter, the discrete space can be denoted as a vector, $D = (D^1, \ldots, D^N)$. It is not necessary to seek to calculate the function score from all discrete spaces with, because Levenberg-Marquardt method updates the initial x_k^0 to the new parameter, x_k^{new} subject to converge toward to its local optimum. DSLM algorithm marks the spaces between D^k and $D^{k'}$ where x_k^0 and x_k^{new} belong to, respectively. It makes reduction of the spaces to check. The dot lines of Figure 4.1 illustrate the discrete spaces. For example, if Levenberg-Marquardt method converges to -2.2 starting from initial guess parameter, -2.7, it would affect marking two spaces, D^4 and D^5 not to visit them again at Figure 4.1. Unlike other similar algorithms using discretization, DSLM's discretization doesn't affect accuracy of the solution but only for preventing rechecking the space.

4.3.4 Algorithm

The following pseudo-codes, Algorithm 2, 3, and 4 briefly illustrate DSLM algorithm. DSLM starts with randomly chosen initial parameters $\mathbf{x}^0$, which is a vector consists of $\{\mathbf{x}_1, \ldots, \mathbf{x}_n\}$ where n is the number of parameters. It iterates updating $\mathbf{x}$ until $\mathbf{x}$ falls into converge or the number of iteration is bigger than a maximum constant. DSLM ensures $F(\mathbf{x}') \leq F(\mathbf{x})$, where $F(\mathbf{x})$ is the function score with $\mathbf{x}$.

DSLM function, shown at Algorithm 3, is the key of the algorithm. It checks the function scores of discrete spaces updating x_i. N is a pre-defined constant which may cover local curves of the function. $5 - 12$ lines of Algorithm 3 illustrate the optimum selection for each parameter and marking the discrete spaces. The reason to check between $F(x_i')$ and F_{min} is to ensure if x_i' is a selection as a better candidate.

Algorithm 2 Main Iteration

Require: $\epsilon > 0$
1: $\mathbf{x} \leftarrow rand()$
2: **while** $iteration \leq maxIteration$ **do**
3: $\mathbf{x}^{'} = DSLM(\mathbf{x})$
4: **if** $\|(\mathbf{x}^{'} - \mathbf{x})\| < \epsilon$ **then**
5: Break
6: **end if**
7: $\mathbf{x} \leftarrow \mathbf{x}^{'}$
8: $iteration = iteration + 1$
9: **end while**

It is to avoid falling wrong local minima. After selection of all parameters, it conducts LM method to get its comprehensive local optimum.

Algorithm 3 DSLM Function

Require: $N > 0$
1: N $\leftarrow$ Number of discretizing the space
2: **for all** i each of **x do**
3: $F_{min} = F(x_i)$
4: $M \leftarrow Array(N)$
5: **while** Not IsAllMarked(M) **do**
6: $x_i \leftarrow$ uniformly random variable among unmarked space of M
7: $\mathbf{x}^{'} = LM(\mathbf{x})$
8: Mark M between$(x_i, x_i^{'})$
9: **if** $F(x_i^{'}) < F_{min}$ **then**
10: $\mathbf{x} \leftarrow \mathbf{x}^{'}$
11: **end if**
12: **end while**
13: **end for**
14: $\mathbf{x} = LM(\mathbf{x})$
15: **return x**

LM method is implemented as George, Sam and Ting proposed [15]. λ is a damping parameter decided by τ and $\max(diag(H))$ [16]. If $\lambda \gg 0$, it behaves like the steepest descent direction method, and performs like Gauss-Newton method if

Algorithm 4 LM Function

1: **while** $iteration \leq maxIteration$ **do**
2: $H \leftarrow J(x)^\top J(x)$
3: $\lambda \leftarrow \tau \max(diag(H))$
4: Solve $(H + \lambda diag(H)) \triangle \mathbf{x} = J(x)^\top F(\mathbf{x})$
5: **if** $F(\mathbf{x} + \triangle \mathbf{x}) < F(\mathbf{x})$ **then**
6: $\mathbf{x} \leftarrow \mathbf{x} + \triangle \mathbf{x}$
7: $\tau \leftarrow \tau / c_1$
8: $iteration \leftarrow iteration + 1$
9: **else**
10: $\tau \leftarrow \tau \times c_2$
11: **end if**
12: **end while**
13: **return** $\mathbf{x}$

λ is zero. In 5-11 lines of Algorithm 4, it adjusts λ depends on the function score, $F(\mathbf{x} + \triangle \mathbf{x})$. If the result of the new parameter is better, it decreases λ to converge quickly to the optimum. Otherwise, it adjusts λ to move slowly to the optimum for smooth curves.

Another issue of the non-linear least squares problem is how to solve inverse as shown at the line 4 of Algorithm 4 because it may cause a problem if it is singular matrix or rank deficient.

$$\triangle \mathbf{x} = (H + \lambda diag(H))^{-1} J(x)^\top F(\mathbf{x}) \tag{4.15}$$

In this thesis, Singular value decomposition(SVD) is used to solve inverse. Briefly, the pseudo-inverse of a vector M (4.16) is calculated by (4.17).

$$M = U \Sigma V^* \tag{4.16}$$

where U is a unitary matrix, Σ is diagonal matrix with non-negative real numbers, V^* is a conjugate transpose of V, which is a unitary matrix.

$$M^+ = V\Sigma^+U^* \tag{4.17}$$

where Σ^+ is the pseudo-inverse of Σ, U^* is a conjugate transpose of U. SVD had better performance compare to QR decomposition and Cholesky decomposition in the experiment.

4.3.5 Derivative of Selection

In this section, we would suggest another approach for selection. In DSLM, selection is computed by choosing the best among scores of the discrete spaces in the selected parameter dimension. Denote $F_{x_i}(x)$ is the score function of selected parameter x_i. If F_{x_i} in the selected parameter's space is convex as following equation, the algorithm can be more simple.

$$F_{x_i}(tx + (1-t)y) \leq tF_{x_i}(x) + (1-t)F_{x_i}(y) \tag{4.18}$$

In this case, it doesn't need to check all of discrete space. As shown following Algorithm 5, the algorithm, first of all, seeks to check the function score for middle of unmarked space. Then, with the comparison between x_i and $x_i^{'}$, it marks a half side of the entire unmarked space. It is supposed that $F(x_i^{'})$ is smaller than $F(x_i)$ by the property of LM algorithm.

Algorithm 5 Another Approach of DSLM Function

Require: $N > 0$

N $\leftarrow$ Number of discretizing the space
for all i each of **x do**
  $F_{min} = F(x_i)$
  $M \leftarrow Array(N)$
  while Not IsAllMarked(M) **do**
    $x_i \leftarrow$ middle of unmarked M space.
    $\mathbf{x}^{'} = LM(\mathbf{x})$
    if $x_i > x_i^{'}$ **then**
      Mark M between(begin of M, $x_i^{'}$)
    else
      Mark M between($x_i^{'}$, end of M)
    end if
    if $F(x_i^{'}) < F_{min}$ **then**
      $\mathbf{x} \leftarrow \mathbf{x}^{'}$
    end if
  end while
end for
$\mathbf{x} = LM(\mathbf{x})$
return x

CHAPTER 5

EXPERIMENTS AND RESULTS

5.1 Preprocessing

Unfortunately, the experiment data of Tang et al [3] is sparse. Sparse observation data may cause inaccurate result of parameter estimation. Also it may have measurement error. Therefore, it needs approaches to deal with a situation. In this section, we provide a method to generate synthetic data to compensate the limitation of available experiment data. The experiment data for this thesis is restricted to estimate parameters of the system without bias. In addition, the data has numerous outliers which cause inconsistent observation, due to small sample size. By generating synthetic data, we can have not only supplementary data to provide more reasonable result, but also consistent data with naturally removed outliers. To generate the synthetic data, Iterative Weighted Mean algorithm is used to remove outliers and to get more accurate mean.

5.1.1 Iterative Wighted Mean Algorithm

While arithmetic mean assumes same weight for each variable, Iterative Weighted Mean method calculates the mean using adaptive weight:

$$\mu_i = \frac{\sum_{i=1}^{n} w_i x_i}{\sum_{i=1}^{n} w_i}, \tag{5.1}$$

where w_i is,

$$w_i = e^{-\frac{(y_i - \mu_{i-1})^2}{\varsigma^2}} \tag{5.2}$$

Here, normal distribution with previous mean, μ_i and variance, σ^2, is used to determine the weight. It iterates until w_i - w_{i-1} goes under a sufficiently small constant ϵ because the mean will be changed due to the weight's update. It is described in Algorithm 6. The initial mean starts with arithmetic mean, but it updates to a more precise mean considering weight. After getting the mean matrix, the synthetic data is generated by normal distribution with the mean finally calculated by iterative weighted mean and the variance of original data to mimic as much as possible the original dispersion. Then, it linearly interpolates for every discrete time. As a result, the synthetic data is generated naturally combining with the original data as shown at Figure 5.1. As more synthetic data is generated, the condensability of the data, which is close to the weighted mean calculated by iterative weighted mean method, will be increasing. It causes naturally reducing outlier's weight.

Algorithm 6 Pseudocode of Iterative Weighted Mean

1: $error \leftarrow \inf$
2: $M \leftarrow \frac{\sum X}{n}$
3: **while** $error > \epsilon$ **do**
4: $\quad w_{new} \leftarrow e^{\frac{(X-M)^2}{\sigma^2}}$
5: $\quad error \leftarrow \sum (w_{new} - w_{old})^2$
6: $\quad w_{old} \leftarrow w_{new}$
7: $\quad M \leftarrow \frac{\sum Xw}{\sum w}$
8: **end while**

Table 5.1: DSLM Computation Results of Each Iteration for Residual Histamine.

Iteration	F(x) with initial β	F(x) with finally updated β
#1	637780.095482	130627.383797
#5	130627.383797	78321.652563
#10	78321.652563	66842.784659
#15	66842.784659	53507.824805
⋮	⋮	⋮
#103	39638.055401	35718.505982

5.2 Parameter Estimation for Residual Histamine

The parameter estimation for residual histamine - (3.7), (3.8), (3.9), and (3.10), is computed by DSLM method implemented by MATLAB R2008a. Totally seven unknown parameters - $\beta, t_1, k_{e0}, k_{k1}, k_{w0}, k_{k2}, k_{rhch}$, are estimated, given 100 synthetic data set. Figure 5.2 and Table 5.1 illustrate the processes that DSLM converges to the optimums for each iteration. For each iteration, DSLM starts its computing with initial parameters (Red lines), and it finally converges to the final optimums of the iteration (Blue lines). Observation data set is depicted by its mean and standard deviation for convenient comparison between estimation and observation. In conclusion, DSLM estimation converged quickly in the beginning of the iterations, as shown at Figure 5.2. Then, it stopped after meeting the convergence criteria. Figure 5.3 shows final result of the experiment after 103 iterations. Estimation for all parameters are listed at Table 5.2.

5.3 Parameter Estimation for Phagocyte

For phagocyte simulation, 15 parameters - k_{hs}, k_{hchrb}, k_{hchrt}, k_{hrs}, k_{hcsb}, k_{hcst}, k_{ss}, k_{pmnipb}, k_{pmnipt}, k_{pmnps}, k_{mpipb}, k_{mpipt}, k_{mpps}, k_{pmns}, and k_{mps} of Equation (3.11), (3.12), (3.13), (3.14), (3.15), (3.16), and (3.17) are estimated by DSLM. The parameter k_{rhch} of Equation (3.11) is determined by the result of estimation for residual

Table 5.2: Estimated Parameters for Residual Histamine

Parameter	Description	Estimation
t_1	The starting point that external source is released	3.5000
k_{e0}	The initial concentration of eternal source	11.2464
k_{k1}	Self contraction of external source	0.1017
β	The initial concentration of oscillation bound	0.0134
k_{w0}	The initial value of oscillation frequency	1.4037
k_{k2}	The contraction rate of oscillation frequency	0.0937
k_{rhch}	Rate that Residual histamine decayed	0.3704

histamine. This dynamic system consists of consecutive seven equations mutually affecting each other, and Figure 5.4 shows the observation data sets of PMN and MΦ.

The results for each iterations of DSLM method are shown in Figure 5.5 and Figure 5.6. As starting with random initial variables, it moved quietly fast to the more optimized space. In conclusion, Figure 5.7 illustrates the final result of DSLM computing after 60 iterations. However, it seems that the optimal estimated figure does exactly not match the observation data set. This result of imperfect matching may be caused by measurement error or undiscovered components that actually affect the phenomenon.

The result of optimal estimation for parameter on phagocyte transmigration is listed in Table 5.3. According to the result, we can verify the half life of histamine is relatively short comparing to others as reported in current biological literature.

5.4 Validation

Although parameter estimation is conducted under the assumption that the mathematic equations of the system represent a true model to cover all phenomenon of the system. However, the biology system is too complicate to model precisely.

Table 5.3: Estimated Optimal Parameters for Phagocyte

Parameter	Description	Estimation
k_{hs}	Rate that histamine regulates itself	0.0002
k_{hchrb}	rate that histamine receptors are released	0.9997
k_{hchrt}	Upper bound rate that histamine receptors are released	0.0757
k_{hrs}	Rate that histamine receptors regulate themselves	0.7232
k_{hcsb}	rate that selectins are released	1.9997
k_{hcst}	Upper bound rate that selectins are released	0.2668
k_{ss}	Rate that selectins regulate themselves	0.1024
k_{pmnipb}	Increasing rate of permeability for PMN	0.2226
k_{pmnipt}	Increasing upper bound rate of permeability for PMN	2.0000
k_{pmnps}	Rate that permeability of capillary self contraction	0.1003
k_{mpipb}	Increasing rate of permeability for MΦ	0.0001
k_{mpipt}	Increasing upper bound rate of permeability for MΦ	1.0108
k_{mpps}	Rate that permeability of capillary self contraction	0.1961
k_{pmns}	Rate that PMN self contraction	0.0582
k_{mps}	Rate that MΦ self contraction	0.0307

Moreover, the exact parameters are not known literately in the biology domain and there may be other unknown components play an important role in the system due to its complexity. For these reasons, validation of DSLM algorithm is difficult for the real system.

For accurate validation of DSLM algorithm, MCMC method is used. The optimal parameters are already estimated in the last section. Synthetic data set can be constructed from the given model, which consists of model equations and estimated parameters. Then, it can verify DSLM performance by matching between previously estimated parameters and DSLM's result with synthetic data.

From Table 5.2 and Table 5.3, optimal parameters are chosen for the true system. Then, it generates synthetic data with certain errors determined by Normal distribution. In this experiment, two data sets are generated by normal distribution

Table 5.4: Result of DSLM Computation for Residual Histamine at The Variance is 0.01 or 0.1.

Parameter	$\sigma = 0.01$	Error ($\lvert\frac{(True-Est)}{True}\rvert$)	$\sigma = 0.1$	Error ($\lvert\frac{(True-Est)}{True}\rvert$)
t_1	3.7600	0.0743	4.2115	0.2033
k_{e0}	0.3699	0.0013	0.3693	0.0030
k_{k1}	17.6195	0.5667	15.2499	0.3560
k_{β}	0.0340	0.6657	0.0555	0.4543
k_{w0}	0.0107	0.2015	0.0199	0.4851
k_{k2}	1.8803	0.3395	2.4857	0.7708
k_{rhch}	0.4381	3.6756	0.4979	4.3138

Table 5.5: Result of DSLM Computation for Phagocyte at The Variance is 0.01 or 0.1

Parameter	$\sigma = 0.01$	Error ($\lvert\frac{(True-Estimate)}{True}\rvert$)	$\sigma = 0.1$	Error ($\lvert\frac{(True-Estimate)}{True}\rvert$)
k_{hs}	1.9894	9946.0000	1.9984	9991.0000
k_{hchrb}	1.4708	0.4712	1.4980	0.4984
k_{hchrt}	0.0541	0.2853	0.1891	1.4974
k_{hrs}	0.0895	0.8762	0.0816	0.8871
k_{hcsb}	1.9685	0.0156	1.9979	0.0000
k_{hcst}	0.1608	0.3973	0.3852	0.4437
k_{ss}	0.0671	0.3447	0.0042	0.9589
k_{ippmnb}	0.0558	0.7493	0.3426	0.5390
k_{ippmnt}	0.9999	0.5000	1.0000	0.5000
k_{pspmn}	0.0718	0.2841	0.0519	0.4825
k_{pmns}	0.0627	0.0773	0.1055	0.8127

where means are from model equations and optimal parameters, and variance (σ) is chosen as 0.01 or 0.1 as shown in Figure 5.8.

By DSLM method, the optimal parameters are calculated as the following results, shown in Table 5.4, Table 5.5, Figure 5.9, and Figure 5.10.

5.4.1 Rastrigin Function

Rastrigin function is a non-convex function for benchmark problems in testing global optimization solution, which is a non-linear multi-modal function with several

local minima. Rastrigin function is used to test DSLM's performance and to verify its expansion.

Rastrigin function is defined by

$$f(\mathbf{x}) = 10n + \sum_{i=1}^{n} x_i^2 - 10\cos(2\pi x_i), \tag{5.3}$$

where n is the number of variables, $-5.12 \leq x_i \leq 5.12, i = 1, 2, \ldots, n$. A variety of dimensions for the function are used for a more complex function to test DSLM method. The global minima for Rastrigin function is known as $x^* = (0, \ldots, 0)$, and minimum score is 0. Rastrigin function with two dimensions is depicted at Figure 5.11.

Global minimal optimization for three numbers of dimensions - 2, 5, and 50 - for Rastrigin function are computed. Figure 5.12(a) illustrates the paths that DSLM takes to find the minimum. It found the approximate solution after only the first iteration. For a five dimensional function, the solution of DSLM approach is very close to the true solution of the function after only 3^{th} iteration as shown at Figure 5.12(d) and 5.12(e). For 50 dimensions, the computation time takes much longer than 5 dimension's, but the performance was still quick and accurate. The true minimum score for the function is 0 for any number of dimensions, and the result by DSLM was 0.0000093, 0.00179665, and 0.0531253 for 2, 5, and 50 dimensional function, respectively. Figure 5.12 shows the transition of parameters and the score for each iteration at n is 2, 5, or 50.

5.4.2 Michalewics Function

Michalewics function is another multi-modal test function defined by

$$f(\mathbf{x}) = -\sum_{i=1}^{n} \sin(x_i)(\sin(\frac{ix_i^2}{\pi}))^{2m} \tag{5.4}$$

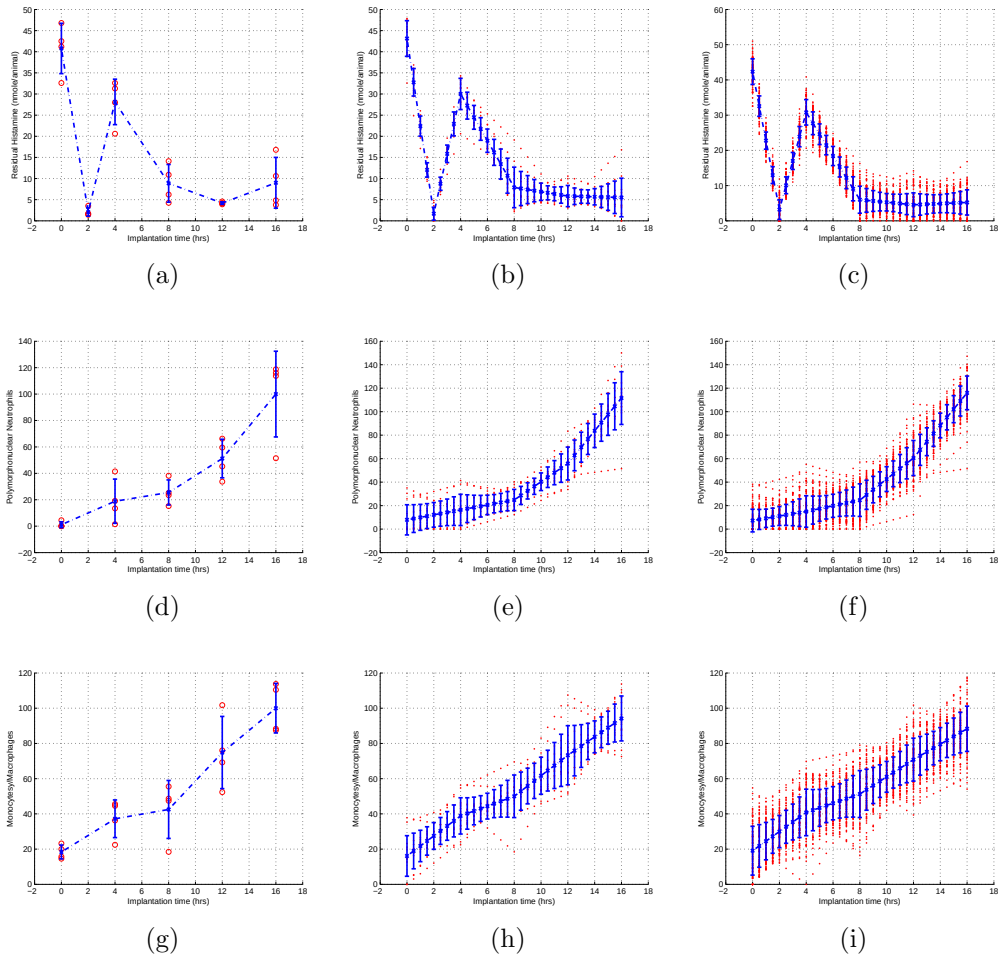

Figure 5.1: Generation of Synthetic Data. Green Dots Illustrate n Number of Data; The Blue Error Bar Describes Mean and Standard Deviation for Each Discrete Time.(a)original observation data for residual histamine; (b)add 10 synthetic data sets; (c)add 100 synthetic data sets; (d)original observation data for PMN; (e)add 10 synthetic data sets; (f)add 100 synthetic data sets; (g)original observation data for MΦ; (h)add 10 synthetic data sets; (i)add 100 synthetic data sets.

Table 5.6: Result of DSLM Computation for Rastrigin Function

Parameter	Estimated(n=2)	Estimated(n=5)	x^*
x_1	0.0000	-0.0003035	0.0000
x_2	0.0002	0.0003219	0.0000
x_3	-	-0.0003534	0.0000
x_4	-	0.0005166	0.0000
x_5	-	-0.0004815	0.0000

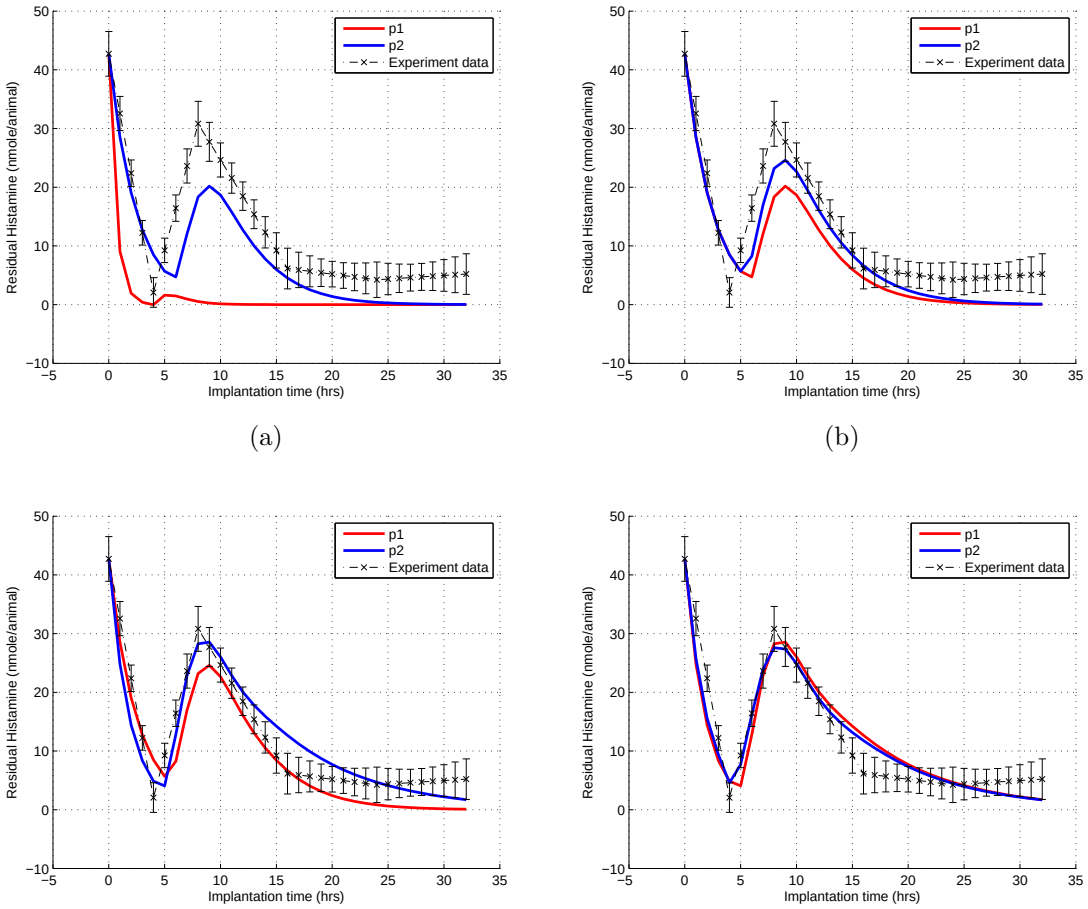

Figure 5.2: Computation Results of Each Iteration for Residual Histamine. (a)the first iteration; (b)the second iteration; (c)the third iteration; (d)the fourth iteration.

where $0 \leq x_i \leq \pi, i = 1, 2, \ldots, n$. m is the "steepness" of the valleys. If m is very large, the valley becomes too sharp to find the minimum. Here, m is set by 10. Michalewics function (m = 10, k = 2, 5, 10) is used to test DSLM method.

As shown as Figure 5.14, the solution of DSLM is reasonably close to the solution. The true solution of function is known as -1.8013 at k = 2, -4.687658 at k = 5, and -9.66015 at k = 10. The result by DSLM for 2, 5, 10 dimensional function was

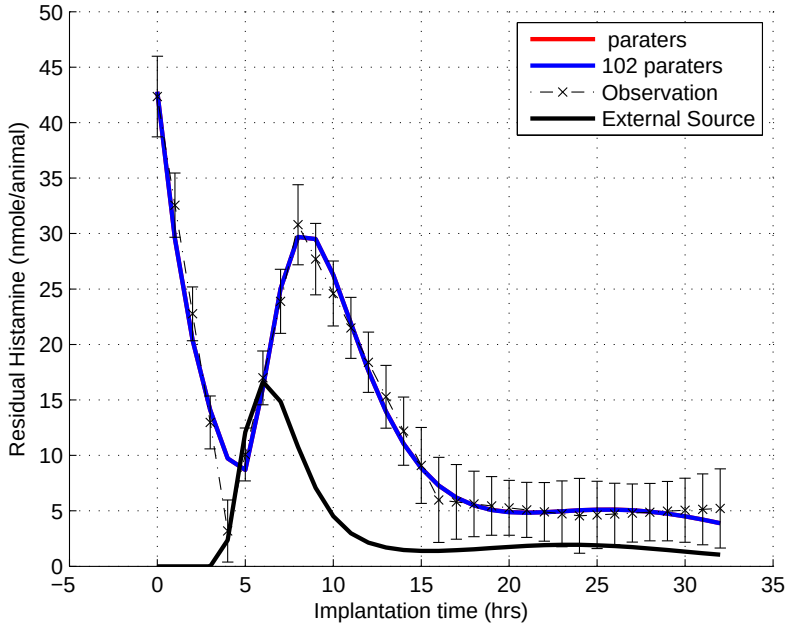

Figure 5.3: Final Result for Residual Histamine

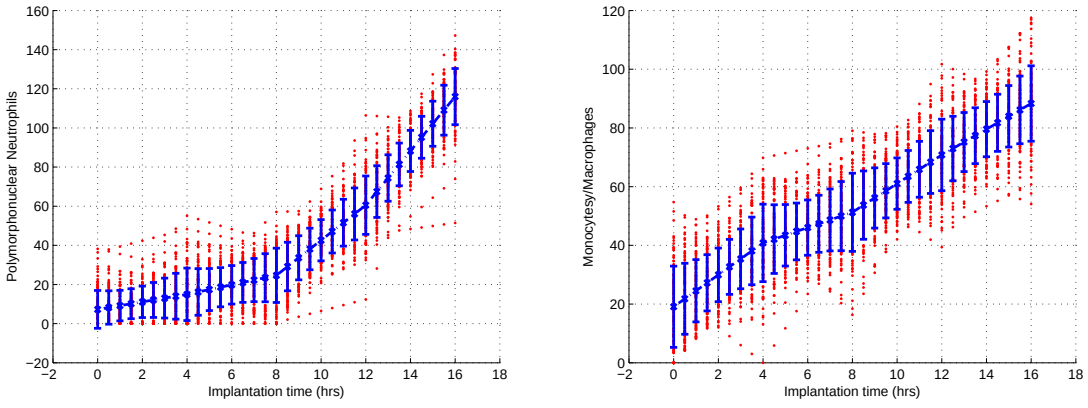

(a) (b)

Figure 5.4: Observation Data Set for PMN and MΦ. (a)data set for PMN; (b)data set for MΦ.

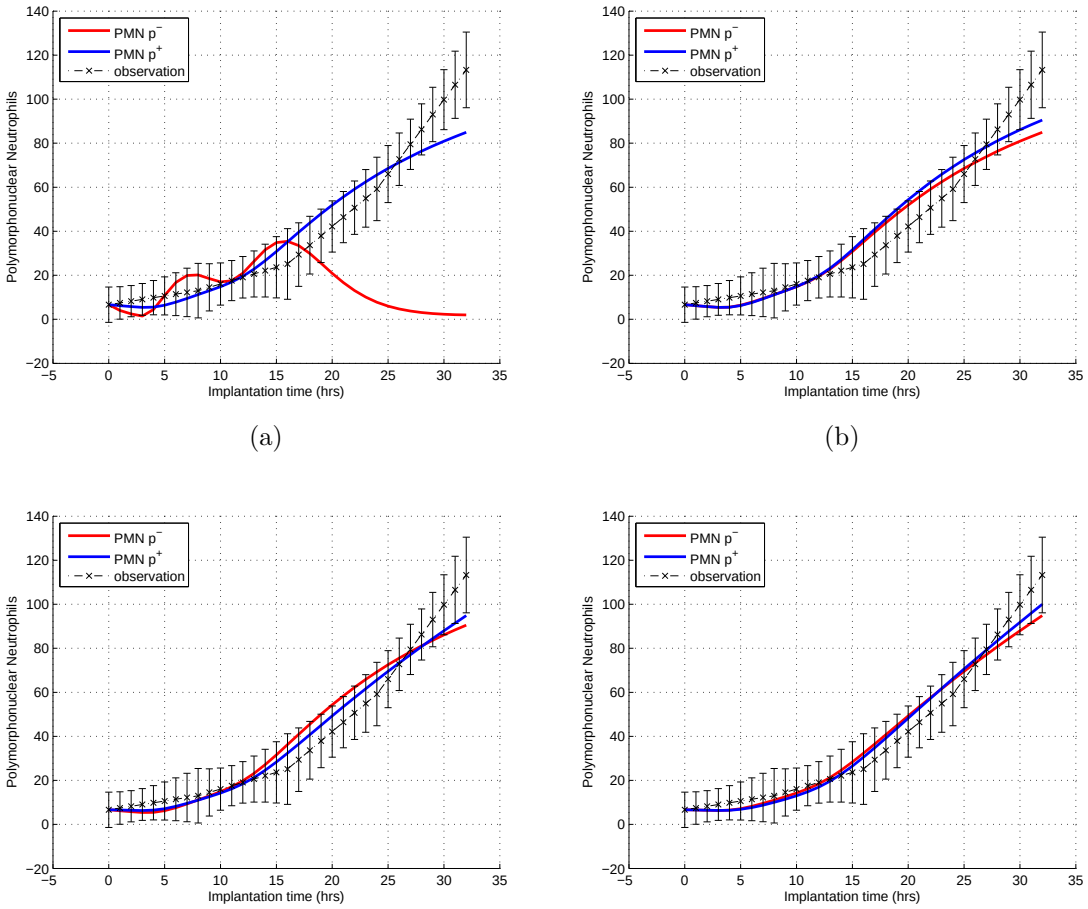

Figure 5.5: DSLM Computation Results of Each Iteration for PMN. (a)the first iteration; (b)the second iteration; (c)the third iteration; (d)the fourth iteration.

-1.801301, -4.687607, and -9.659933 respectively. Figure 5.14 and Table 5.7 show the result in detail.

5.5 Mast Cell Deficiency

The experiment to observe the phenomenon of phagocyte transmigration when mast cells are blocked, was conducted[3]. In this section, we will simulate how much mast cell deficiency influences the whole mechanism of phagocyte transmigration. All

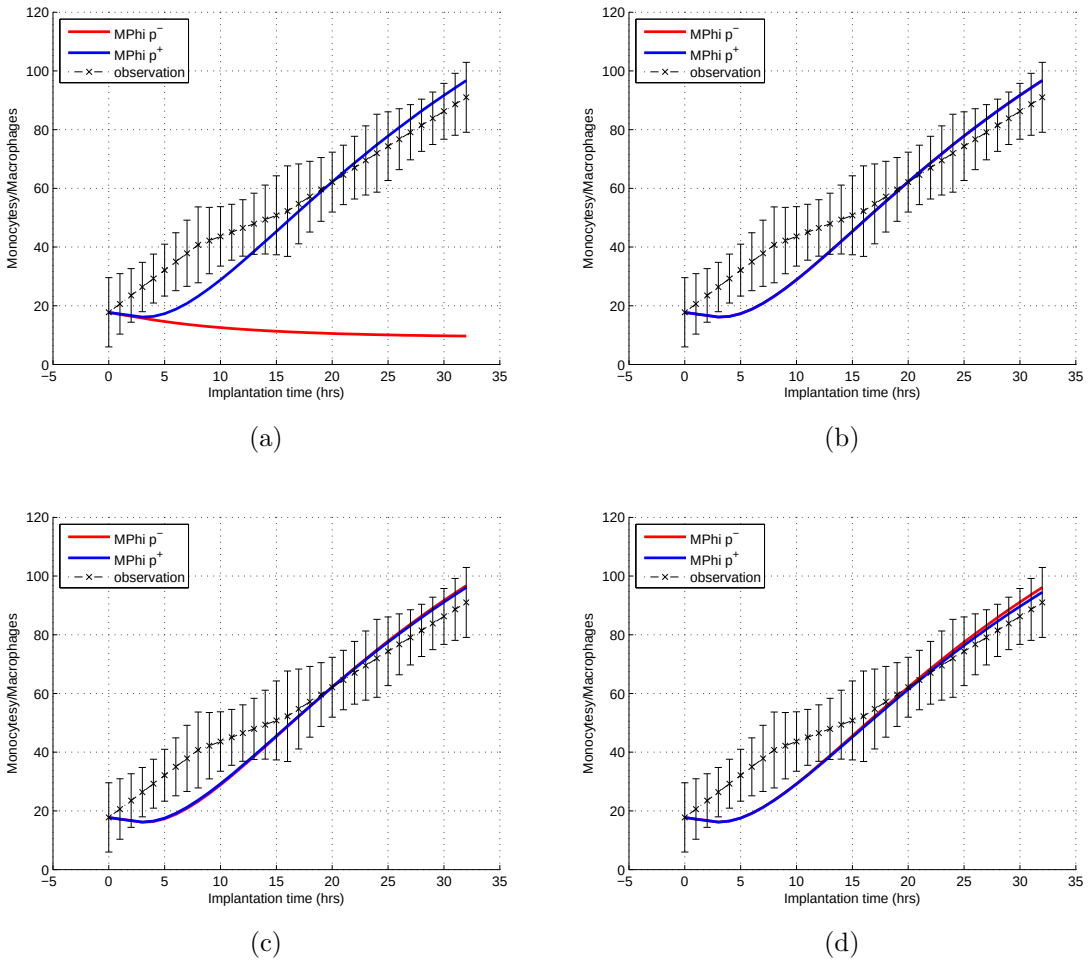

Figure 5.6: DSLM Computation Results of Each Iteration for MΦ. (a)the first iteration; (b)the second iteration; (c)the third iteration; (d)the fourth iteration.

Table 5.7: Result of DSLM Computation for Michalewics Function

Parameter	Estimated(k = 2)	Estimated(k = 5)
x_1	2.2026602	-0.0003035
x_2	1.5706679	0.0003219
x_3	-	-0.0003534
x_4	-	0.0005166
x_5	-	-0.0004815

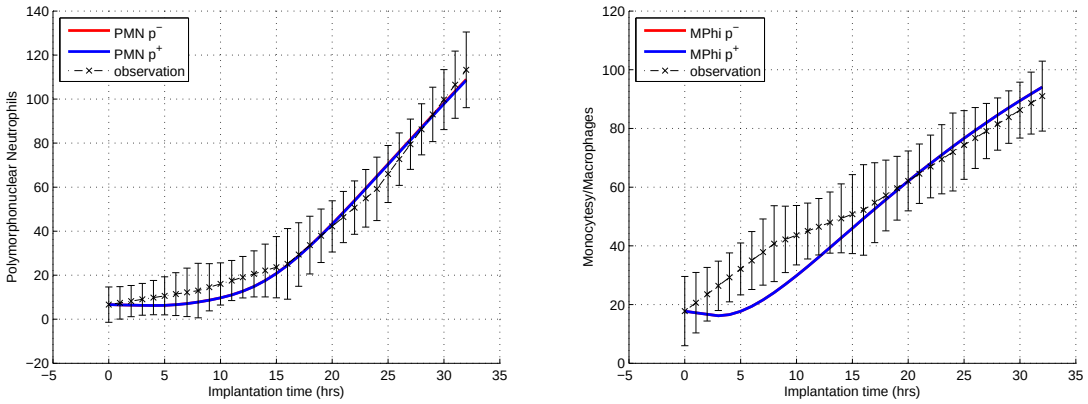

(a) (b)

Figure 5.7: The Final Results for PMN and MΦ. (a)final Result for PMN; (b)final Result for MΦ.

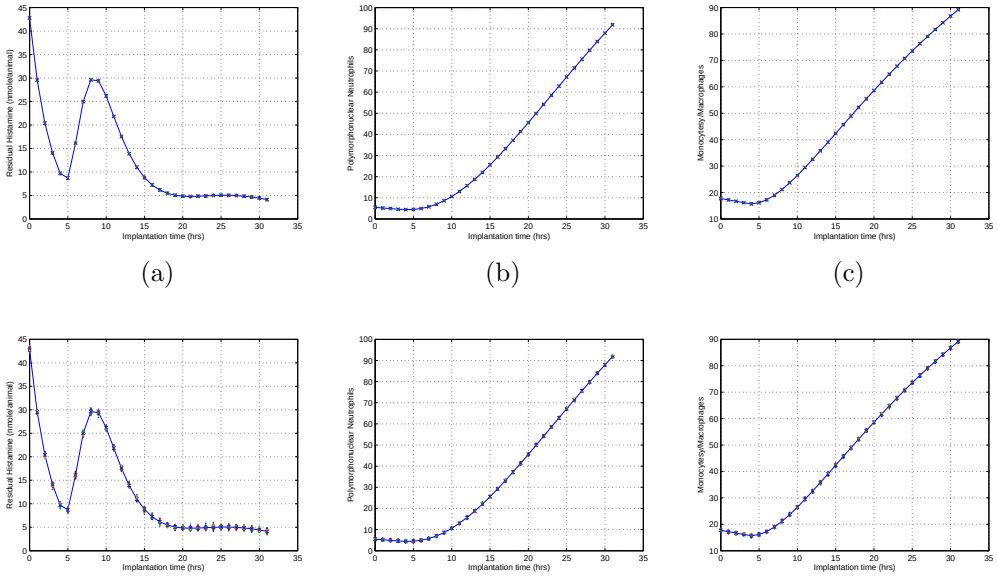

(a) (b) (c)

(d) (e) (f)

Figure 5.8: Synthetic Data Set of PMN and MΦ for Validation. (a)data set, $\sigma = 0.01$ for residual histamine; (b)data set, $\sigma = 0.01$ for PMN; (c)data set, $\sigma = 0.01$ for MΦ; (d)data set, $\sigma = 0.1$ for residual histamine; (e)data set, $\sigma = 0.1$ for PMN; (f)data set, $\sigma = 0.1$ for MΦ.

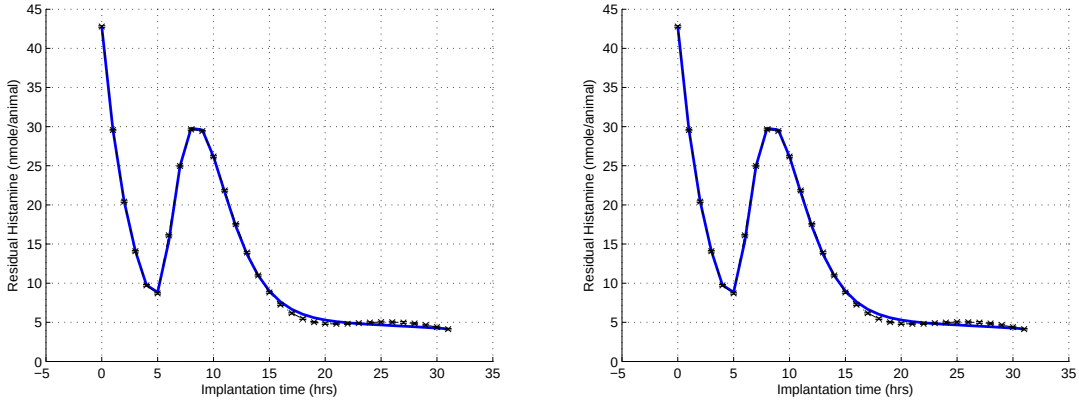

(a) (b)

Figure 5.9: Result of DSLM Method for Residual Histamine. (a)$\sigma = 0.01$; (b)$\sigma = 0.1$.

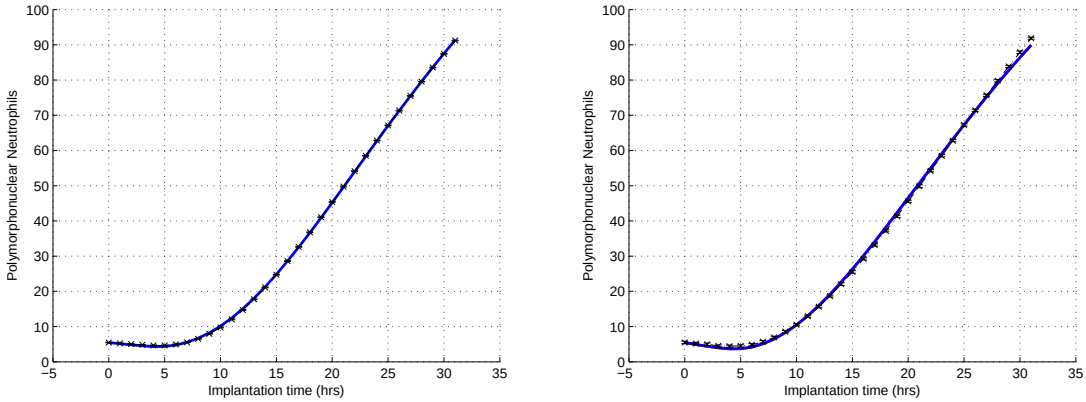

(a) (b)

Figure 5.10: Result of DSLM Method for Phagocyte. (a)$\sigma = 0.01$; (b)$\sigma = 0.1$.

Table 5.8: Total Recruited PMN on Mast Cell Deficiency

	#1	#2	#3	#4	#5
Control	2828.171091	2539.085546	2424.041298	3905.60472	6463.864307
Deficient	1289.085546	1693.215339	1433.628319	1865.781711	942.4778761

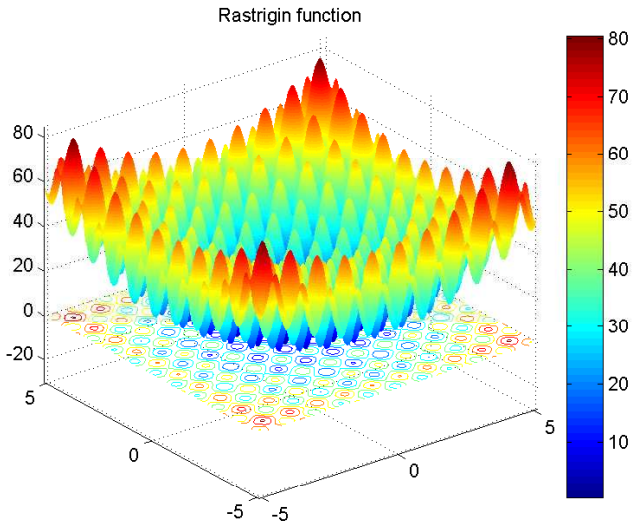

Figure 5.11: Rastrigin function. $x^* = (0, \ldots, 0), f(x^*) = 0$

parameters of the system are known or optimally estimated under the control condition, i.e, parameters are adopted from Table 5.2 and Table 5.3. Under the assumption that estimated parameters represent the true system appropriately no matter what any exceptional conditions, the coefficient constant is computed. Table 5.8 shows totally accumulated PMN of mast cell deficient mice after 16 hours. Here, it is calibrated to be proportional to the ratio of PMN simulated for the 16 hour by computation. Mast cell deficiency is represented I_{mc} in Equation (3.11), where I_{mc} is 1 for control, and $0 \leq I_{mc} \leq 1$ for Mast cell deficiency.

$$I_{mc} = \begin{cases} 1 & \text{Control;} \\ I_{mc} & 0 \leq I_{mc} \leq 1 \text{ for Mast Cell deficiency.} \end{cases} \tag{5.5}$$

Since (3.11) which is convex for I_{mc}, the parameter estimation is computed by general Levenberg-Marquardt Algorithm. The results for mast cell deficiency are described in Figure 5.15 and Figure 5.16, and optimal I_{mc} was computed as 0.0219. Here,

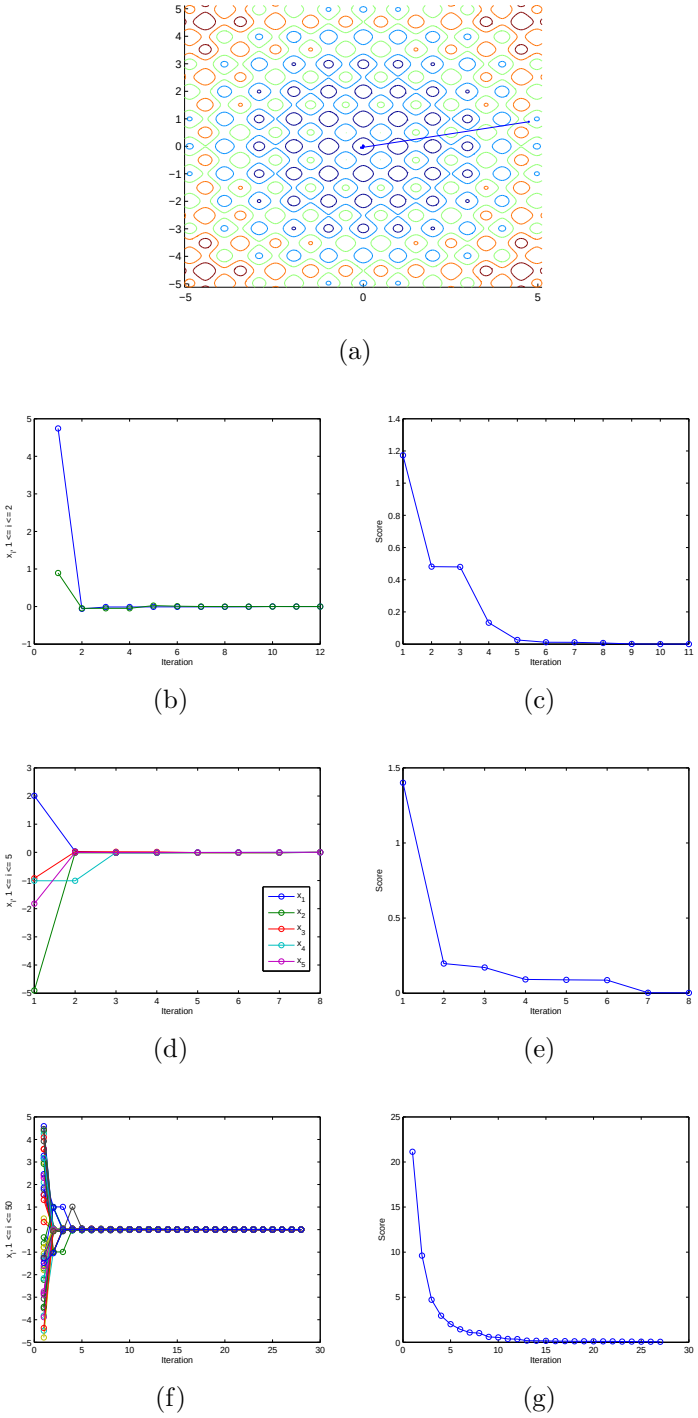

Figure 5.12: Result for A Variety of Dimensional Rastrigin Function (a)the paths that DSLM takes to find the minimum for 2 dimensional function; (b)parameters at k = 2; (c)scores at k = 2, 0.0000093; (d)parameters at k = 5; (e)scores at k = 5, 0.00179665; (f)parameters at k = 50; (g)scores at k = 50, 0.0531253.

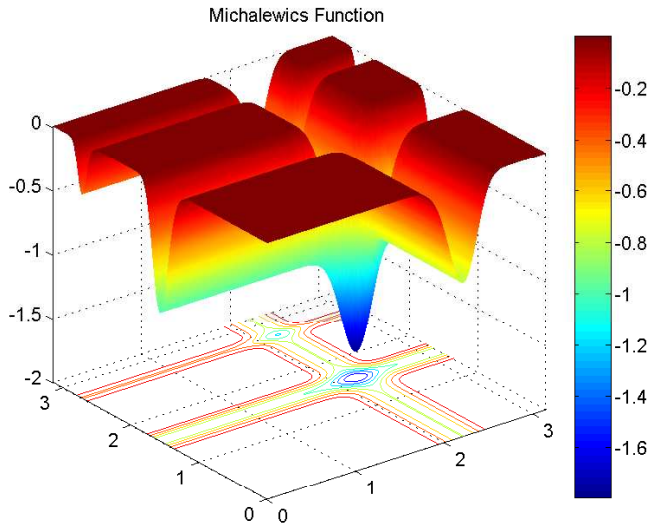

Figure 5.13: Michalewics Function. $f(x^*) = -1.8013$ at k = 2, $f(x^*) = -4.687658$ at k = 5, $f(x^*) = -9.66015$ at k = 10.

the result for MΦ seems unreasonable matching between prediction and observation data. That is because the parameters regarding to MΦ are negligibly low to affect the deficiency of Mast Cells.

5.6 P/E selectins Deficiency

For modeling the system of P/E selectins deficiency used in Equations (3.14) and (3.15), I_{pmns} and I_{mps} are considered as follwoing

$$I_{pmns}, I_{mps} = \begin{cases} 1 & \text{Control;} \\ I_P & 0 \leq I_P \leq 1 \text{ for P selectin deficiency.} \\ I_{P/E} & 0 \leq I_{P/E} \leq 1 \text{ for P/E selectin deficiency.} \end{cases} \tag{5.6}$$

However, only MΦ experiment data is used in this section because the number of reliable PMN measurement is very low and is ignored due to a severe inflammation. Overwhelming macrophages dominate the inflamed tissue at the point. Tables 5.9

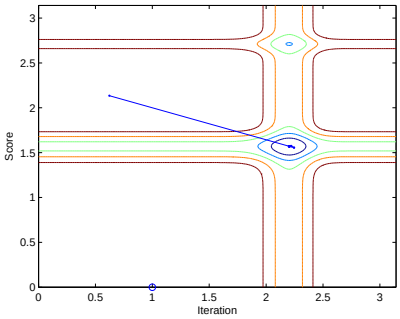

(a)

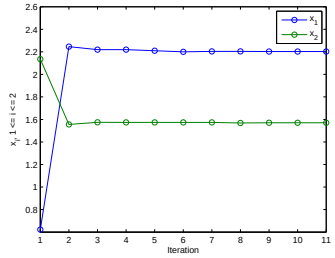

(b)

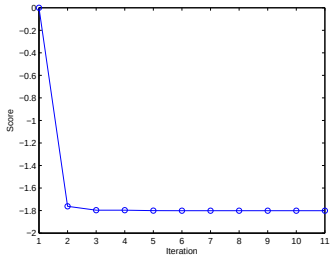

(c)

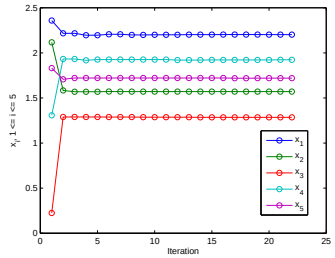

(d)

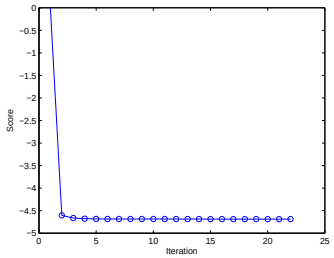

(e)

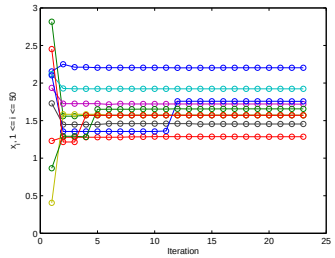

(f)

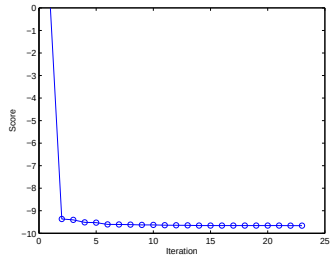

(g)

Figure 5.14: Result for Michalewics Function. (a)the paths that DSLM takes to find the minimum for 2 dimensional function; (b)parameters at k = 2; (c)scores at k = 2, -1.8013; (d)parameters at k = 5; (e)scores at k = 5, -4.6876; (f)parameters at k = 10; (g)scores at k = 10, -9.6599.

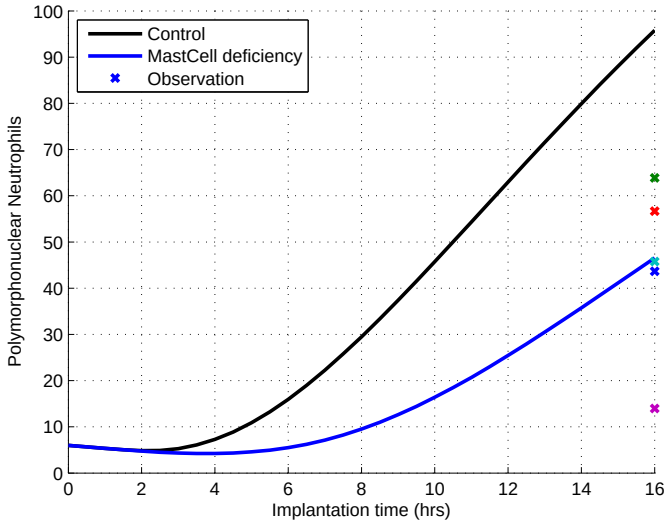

Figure 5.15: Simulation Result of PMN Totally Recruited to Peritoneum Including on Intraperitoneal Implant Surface and Peritoneal Cavity in Mast Cell Deficient Mice after Intraperitoneal Implantation for 16 Hours. Dots at 16 Hour are Real Experiment Data.

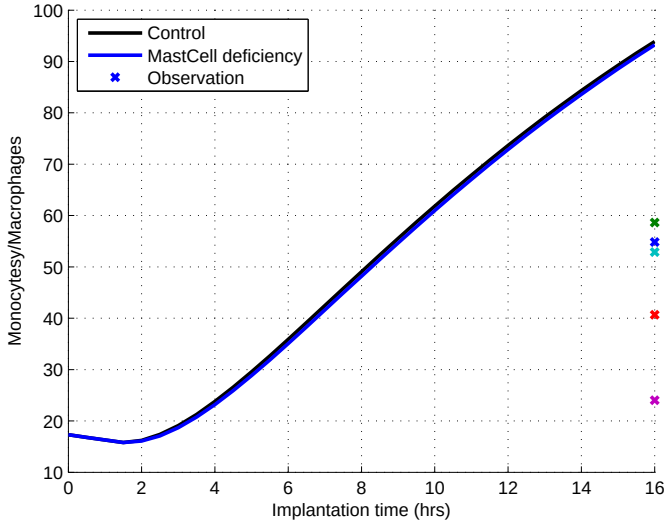

Figure 5.16: Simulation Result of MΦ Totally Recruited to Peritoneum Including on Intraperitoneal Implant Surface and Peritoneal Cavity in Mast Cell Deficient Mice after Intraperitoneal Implantation for 16 Hours. Dots at 16 Hour are Real Experiment Data.

Table 5.9: Total Recruited MΦ on P selectin Deficiency

	#1	#2	#3	#4	#5
Control	179.2548	170.3769	183.8739	151.4317	182.9275
P Deficient	206.2488	175.9381	273.6207	140.5395	111.6484

Table 5.10: Total Recruited MΦ on P/E selectins Deficiency

	#1	#2	#3	#4	#5
Control	204.8366	110.9817	94.8825	195.2455	164.7598
P/E Deficient	67.4796	59.6012	41.1043	40.4192	35.6237

and 5.10 show totally accumulated MΦ of P selectin or P/E selectins deficient mice after 16 hours. For this reason, PMN experiment data for P/E selectins is ignored. The computation results of I_{mps} for P and P/E selectins deficiency are 1.1122, 0.0008, respectively, and the result is illustrated in Figure 5.17.

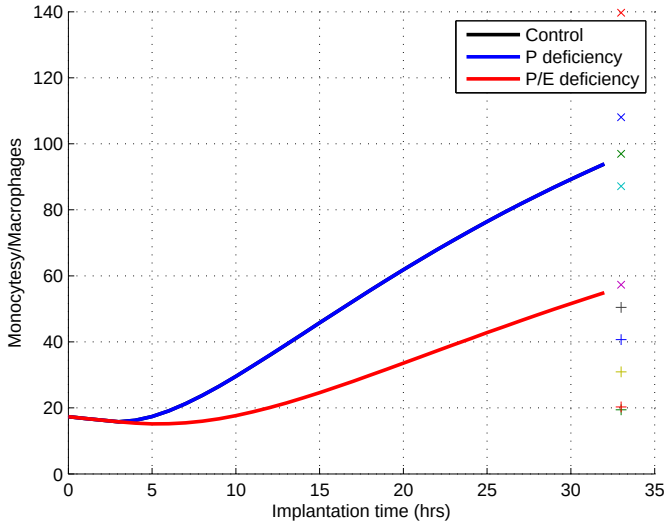

Figure 5.17: Simulation Result of MΦ Totally Recruited on Both Intraperitoneal Implants and Subcutaneous Implants in P and P/E selectins Deficient Mice after Intraperitoneal Implantation for 16 Hours. Dots at 16 Hour are Real Experiment Data.

5.7 H1/H2 Histamine Receptors Deficiency

In Equations (3.14) and (3.15), I_{pmnhr} and I_{mphr} represent inputs of indicating blocking out H1, H2, and H1/H2 Histamine Receptors.

$$I_{pmnhr}, I_{mphr} = \begin{cases} 1 & \text{Control} \\ I_{h1} & \text{H1 histamine receptor deficiency} \\ I_{h2} & \text{H2 histamine receptor deficiency} \\ I_{h1h2} & \text{H1/H2 histamine receptor deficiency} \end{cases} \tag{5.7}$$

Table 5.11 and Table 5.12 list the observation data set. Same as the estimation for other deficiencies, it is also computed by general Levenberg-Marquardth method. I_{pmnhr} is computed as 0.5447, 0.3865, 0.2116 for H1 histamine receptor, H2 histamine receptor, H1/H2 histamine receptors deficiency, respectively, and I_{mphr} is estimated as 0.0019, 0.0028, and 0.0012, respectively. The results are depicted in Figure 5.18.

Table 5.11: Total Recruited PMN on H1/H2 Histamine Receptors Deficiency

	#1	#2	#3	#4	#5	#6
Control	96.037	111.50	65.34	102.13	127.41	97.56
H1 Deficient	35.18	68.73	47.78	60.50	53.66	53.99
H2 Deficient	32.76	54.60	41.92	11.96	59.69	51.66
H1/H2 Deficient	48.53	25.84	23.53	46.55	66.45	56.46

Table 5.12: Total Recruited MΦ on H1/H2 Histamine Receptors Deficiency

	#1	#2	#3	#4	#5	#6
Control	97.84	116.44	72.76	77.92	135.04	99.97
H1 Deficient	57.93	85.22	58.18	63.42	95.79	80.95
H2 Deficient	76.70	61.29	68.53	109.06	51.29	73.25
H1/H2 Deficient	64.16	63.50	70.05	59.81	72.11	50.31

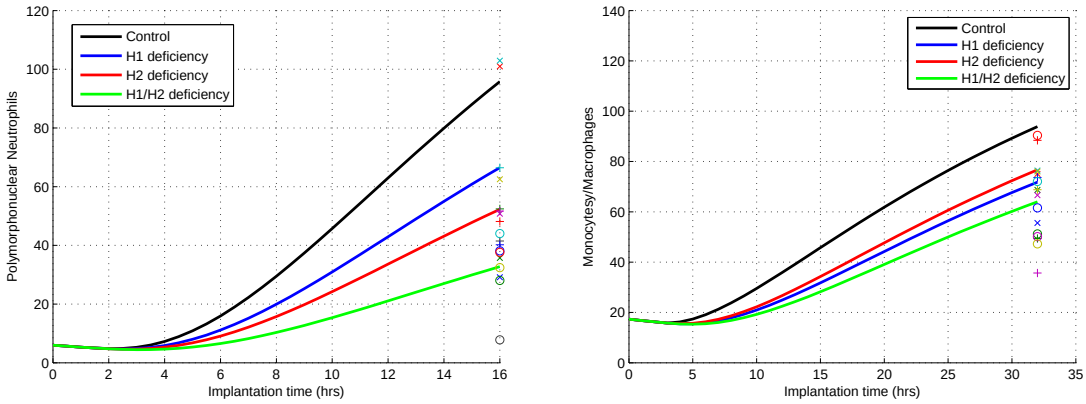

(a) (b)

Figure 5.18: Simulation Result of PMN and MΦ Totally Recruited on Both Intraperitoneal Implants and Subcutaneous Implants in Histamine Receptors(H1 and H2) Deficient Mice after Intraperitoneal Implantation for 16 Hours. Dots at 16 Hour are Real Experiment Data. (a)histamine receptor deficiency Result for PMN; (b)histamine receptor deficiency Result for MΦ.

5.8 Simulation and Prediction

Until now, all parameters for the phagocyte transmigration are estimated. Tables 5.2, 5.3 list the parameter values optimally estimated by DSLM. In this section, the prediction of the system using the complete system model is conducted. For the existing data set, there are only data up to 16 hours, and each data sets was carried out independently from separate experiment such as residual histamine, PMN, MΦ, mast cell deficiency, H1/H2 histamine receptors deficiency, and P/E selectins deficiency. By using the computational model, the simulation of experiments' conditions can be possible, even after 16 hours.

Figures 5.19, 5.20, and 5.21 show the predicted dynamic illustration of recruited residual histamine, PMN, and MΦ up to 36 hours, respectively.

For deficiency simulation, simulation for blocking of mast cells, H1/H2 histamine receptors, and P/E selectins were conducted. Prediction of recruited PMN while blocking mast cells between 0 and 25 hours is illustrated in Figure 5.22. In addition, H1/H2 histamine receptors are blocked after 25 hours, shown as in Figure 5.23. For P/E selectins deficiency simulation, prediction of recruited MΦ for blocking P/E selectins between 0 and 20 hours is shown in Figure 5.24.

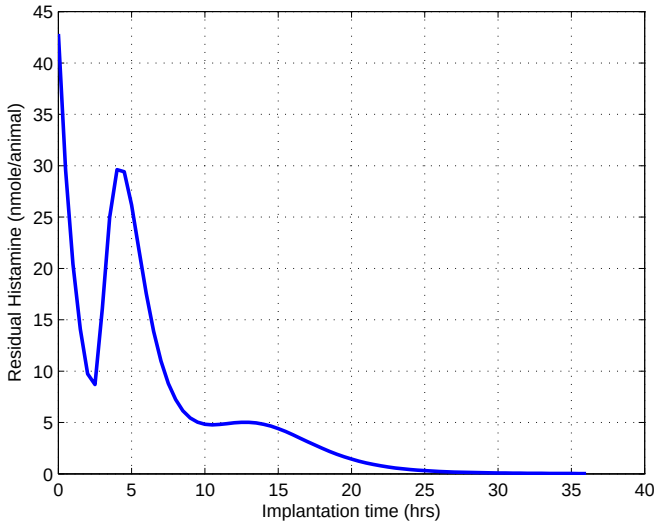

Figure 5.19: Prediction of Residual Histamine up to 36 Hours

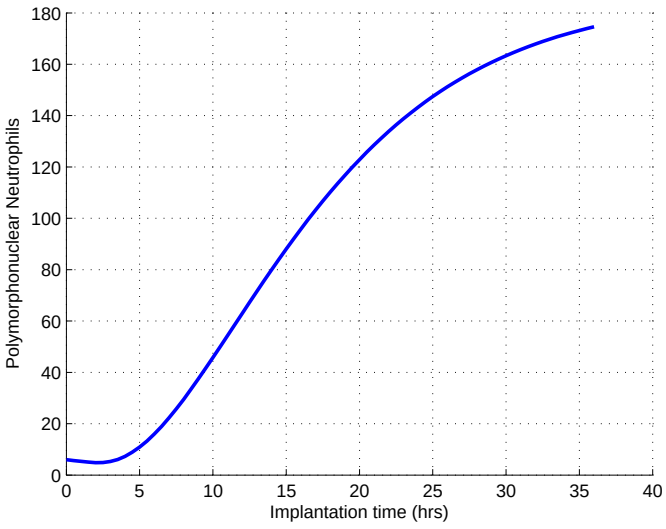

Figure 5.20: Prediction of PMN up to 36 Hours

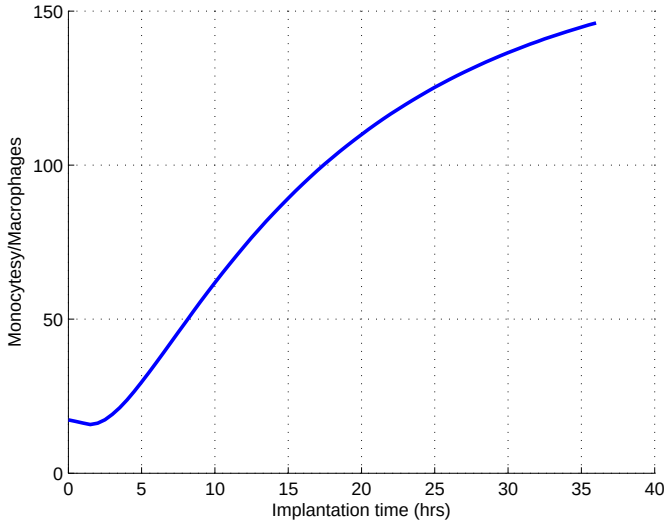

Figure 5.21: Prediction of MΦ up to 36 Hours

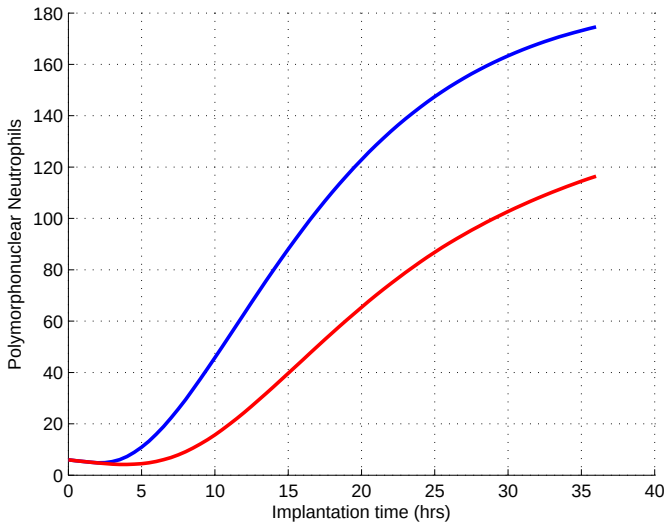

Figure 5.22: Prediction of Recruited PMN (Mast Cell are Blocked Between 0 and 25 Hours).

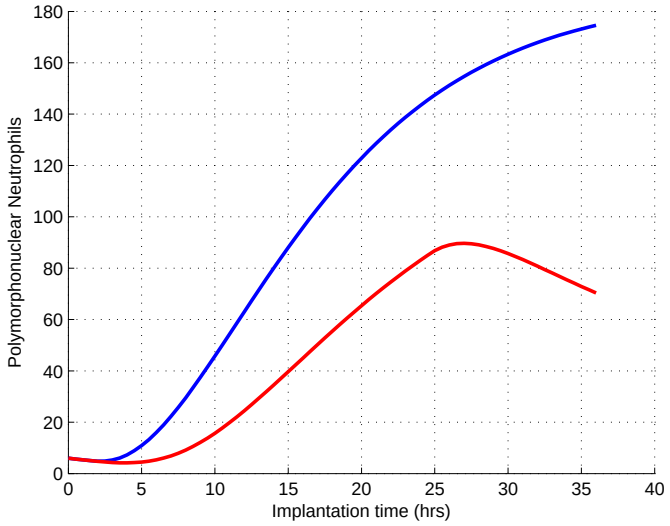

Figure 5.23: Prediction of Recruited PMN (Mast Cells are Blocked Between 0 and 25 Hours, and H1/H2 Histamine Receptors are Blocked after 25 Hours)

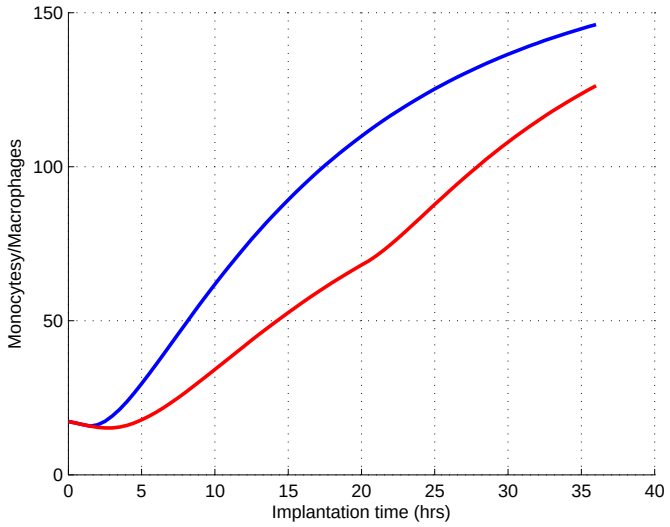

Figure 5.24: Prediction of Recruited MΦ (P/E selectins are Blocked Between 0 and 20 Hours.)

CHAPTER 6

CONCLUSION

Phagocyte transmigration has been studied to tackle the problem of fibrotic tissue formation surrounding the biomaterial implants, which causes implantation failure. To reduce the failure, we modeled phagocyte transmigration using mathematical equations, because in-depth understanding of the system and prediction can control the following events in the implantation phenomenon. To complete the modeling, reverse engineering is conducted to estimate the parameters of the mathematical modeling equations. For parameter estimation, several optimization methods, such as Levenberg-Marquardt algorithm and Genetic algorithm, have been introduced. We proposed a global heuristic optimization technique, DSLM which is designed to overcome the limitations of existing algorithms; LM algorithm is not suitable for global optimal problems and some heuristic global optimizations doesn't guarantee convergence. However, LM algorithm is the most popular and the strongest method to find optimization solution in the local convex space and heuristic searching algorithms provide solutions for global optimization. DSLM adopts both of strength, which are optimal convergence of LM algorithm in the local convex spaces and global selection strategy of Genetic Algorithm. In the experiments of Phagocyte Transmigration, DSLM is performed to optimally estimate the parameters of the model equations. With mathematical equations for system modeling and the estimated parameters by DSLM, Phagocyte Transmigration is simulated. This simulation can be used to predict the future evolution of Phagocyte Transmigration when implantation, and it can be applied for successful implant surgical procedures. Also DSLM can be applied as

global optimization solutions. It is tested with Rastrigin Function and Michalewics Function, which are popular problems, to verify its performance and generality of use.

REFERENCES

[1] L. Christenson, P. Aebischer, P. McMillan, and P. M. Galletti, "Tissue reaction to intraperitoneal polymer implants: species difference and effects of corticoids and doxorubicin," *Jounal of Biomedical Materials Research*, vol. 23, no. 7, pp. 705–18, 1989.

[2] L. Tang, Y. Wu, and R. B. Timmons, "Fibrinogen adsorption and host tissue responses to plasma functionalized surfaces," *Jounal of Biomedical Materials Research*, vol. 42, no. 1, pp. 156–63, 1998.

[3] L. Tang, T. A. Jennings, and J. W. Eaton, "Mast cells mediate acute inflammatory responses to implanted biomaterials," *Proceedings of the National Academy of Sciences*, vol. 95, July 1998.

[4] P. Kuzniar, "Degranulation," *Wikipedia*, 2006. Available: http://en.wikipedia.org/wiki/Degranulation.

[5] T. L, J. W, and W. SE, "The participation of p- and e-selectins on biomaterial-mediated tissue responses," *Jounal of Biomedical Materials Research*, vol. 62, no. 4, pp. 471–477, 2002.

[6] J. Xue, J. Gao, and L. Tang, "Phagocyte transmigration modeling using system dynamic controls," *IEEE International Conference on Bioinformatics&Bioengineering*, pp. 480–485, 2007.

[7] J. Xue, J. Gao, and L. Tang, "A hybrid computational model for phagocyte transmigration," *IEEE International Conference on Bioinformatics&Bioengineering*, pp. 1–6, December 2008.

[8] M. Sutherland, "The damped oscillator," Available: http://www.scar.utoronto.ca/ pat/fun/NEWT1D/PDF/OSCDAMP.PDF.

[9] J. L. Crassidis and J. L. Junkins, *Optimal estimation of dynamic systems*. Chapman & Hall/CRC, 2004.

[10] J. John E. Dennis, D. M. Gay, and R. E. Welsch, "An adaptive nonlinear least-squares algorithm," *ACM Transactions on Mathematical Software*, vol. 7, pp. 348–368, September 1981.

[11] H. B. Nielsen, "Damping parameter in marquardt's method," tech. rep., Department of Mathematical Modeling, May 1999.

[12] J. F. Bonnans, J. C. Gilbert, C. Lemarechal, and C. A. Sagastizabal, *Numerical optimization: theoretical and practical aspects*. Springer, 2006.

[13] K. Levenberg, "A method for the solution of certain non-linear problems in least squares," *Quarterly Journal of Applied Mathmatics*, vol. II, no. 2, pp. 164–168, 1944.

[14] M. D. W., "An algorithm for least-squares estimation of nonlinear parameters," *Journal of the Society for Industrial and Applied Mathematics*, vol. 11, pp. 431–441, June 1963.

[15] G. Tucker, S. Whittle, and T. Wang, "On numerical recovery methods for the inverse problem," August 2006.

[16] M. Bun, "Applications of the levenberg-marquardt algorithm to the inverse problem," October 2009.

BIOGRAPHICAL STATEMENT

Mingon Kang received his B.E. degree in Computer Engineering from Hanyang University, South Korea, in 2006, and his Master of Science in Computer Science and Engineering from The University of Texas at Arlington in Aug 2010. His research interests include bioinformatics, machine learning, and data mining.